
Electronic Thesis and Dissertation Repository

11-23-2023 10:30 AM

Series Expansions of Lambert W and Related Functions

Jacob Imre, *Western University*

Supervisor: Jeffrey, David J., *The University of Western Ontario*

A thesis submitted in partial fulfillment of the requirements for the Master of Science degree in Applied Mathematics

© Jacob Imre 2023

Follow this and additional works at: <https://ir.lib.uwo.ca/etd>



Part of the [Numerical Analysis and Computation Commons](#), and the [Special Functions Commons](#)

Recommended Citation

Imre, Jacob, "Series Expansions of Lambert W and Related Functions" (2023). *Electronic Thesis and Dissertation Repository*. 9841.

<https://ir.lib.uwo.ca/etd/9841>

This Dissertation/Thesis is brought to you for free and open access by Scholarship@Western. It has been accepted for inclusion in Electronic Thesis and Dissertation Repository by an authorized administrator of Scholarship@Western. For more information, please contact wlsadmin@uwo.ca.

Abstract

In the realm of multivalued functions, certain specimens run the risk of being elementary or complex to a fault. The Lambert W function serves as a middle ground in a way, being non-representable by elementary functions yet admitting several properties which have allowed for copious research. W utilizes the inverse of the elementary function xe^x , resulting in a multivalued function with non-elementary connections between its branches. $W_k(z)$, the solution to the equation $z = W_k(z)e^{W_k(z)}$ for a “branch number” $k \in \mathbb{Z}$, has both asymptotic and Taylor series for its various branches.

In recent years, significant effort has been dedicated to exploring the further generalization of these series. The first section of this thesis focuses on the generalization and representation of series for any branch of the Lambert W function. Rather than the principal branch in the real plane, non-principal branches are of most interest. Behaviour of these branches’ approximations is studied near branch cuts and for large-indexed branches. This analysis is supported by both images of curves in domain space and domain-colouring of entire regions.

Subsequent sections will focus on a new class of functions which resemble Lambert W . These share a “fundamental relation” with the Lambert W , enabling the previous series to be generalized even further. The complexity of the nested functions will increase throughout these sections. Initially, functions are utilized that are multivalued in a single, elementary fashion. Later, these will be replaced with functions which have more complex branch behaviour.

Keywords: Lambert W , special functions, asymptotic series

Abstract for a Lay Audience

Back in secondary school, one may have learned about functions in math class. One property that is fundamental to the definition of a function is the so-called “vertical-line test”: a curve represents a function if a vertical line passes through said curve only once. In the same class, one may remember learning about inverses of functions, which “cancel” out the other function and leaves only the input. For example, the function f^{-1} is the inverse of another function f if $f^{-1}(f(x)) = f(f^{-1}(x)) = x$.

When combining these two ideas, some contradictory examples may arise. There has been another oft-forgotten aspect of math not yet mentioned: the horizontal line test. When a horizontal line passes through a curve only once, the corresponding function has an inverse. However, higher-level mathematics ignores this rule for some cases. The Lambert W function is one such case, being the inverse of a function which fails the horizontal line test.

As we must still obey the vertical line test, sections of the Lambert W function are treated as separate entities called “branches”. Due to W being a function which is impossible to write out in simpler terms, we need to represent each branch in another way. This thesis focuses on the use of sums of other functions to approximate the branches of W . In addition, we use the same sums to approximate branches of functions similar to W to lay groundwork for future functions which have branches.

THE UNIVERSITY OF WESTERN ONTARIO
School of Graduate and Postdoctoral Studies

CERTIFICATE OF EXAMINATION

Examiners:

Supervisor:

.....
Dr. R. M. Corless

.....
David J. Jeffrey

.....
Dr. G. Reid

Supervisory Committee:

.....
Dr. P. Yu

The thesis by

Jacob Imre

entitled:

Series Expansions of Lambert W and Related Functions

is accepted in partial fulfillment of the
requirements for the degree of
Masters of Science

.....
Date

.....
Chair of the Thesis Examination Board

Co-Authorship Statement

Chapter 2 of this thesis consists of the following paper:

J. Imre and D. J. Jeffrey. Non-principal Branches of Lambert W. A Tale of 2 Circles. CASC 2023. Volume 14139 of *Lecture Notes in Computer Science*, pages 199-212. Springer, 2023.

Acknowledgements

I would like to acknowledge all the faculty members at Western who helped pave the way for this thesis. My advisor, Dr. David Jeffrey, is one of the experts in the subject of the Lambert W function, along with Dr. Rob Corless. Getting to learn from the experts directly has helped me immensely; this thesis would not be what it is without their research and help.

Additionally, I would like to thank all of my fellow students from MC 213 and MC 105. They have all provided an ear when talking about my research, along with helping me iron out issues with presentations. Getting to hear feedback from my peers has been monumental in helping me find my voice.

Finally, I want to thank to my family and everyone who has helped foster my interest in mathematics. I would not be where I am today without the help of Dr. Ekaterina Shemyakova from The University of Toledo. Nor would I be here if not for the continued encouragement from my family.

Contents

Abstract	i
Abstract for a Lay Audience	ii
Certificate of Examination	iii
Co-Authorship Statement	iv
List of Figures	viii
List of Tables	xi
1 Introduction: Series Over Multivalued Functions	1
1.1 Taylor Series for an Elementary Multifunction	1
1.2 Series Approximations of The Lambert W Function in \mathbb{R}	3
1.3 W and multivalued functions in computer algebra	5
2 Series for non-principal branches	7
2.1 Introduction	7
Definitions	7
2.2 Expansions	8
2.2.1 Branch structure	8
2.2.2 Asymptotic expansions	10
2.2.3 Outline	10
2.3 de Bruijn series for large z	11
2.4 de Bruijn series for small z	14
2.5 A surprising convergence	15
3 Further Notes on Convergence	18
3.1 Optimizing Asymptotic Approximations	18
3.2 Convergence Over the Complex Plane	20
4 A Family of Functions Related to Lambert W	25
4.1 Analysis of Select Functions	25
4.2 The Fundamental Relation and The Lambert Family	27
5 Asymptotic Series Expansions for Members of \mathcal{Q}	29

5.0.1	A Naive Approach	29
5.0.2	Accuracy and Efficiency of Nested Series	33
	The Reciprocal Function	33
	Trigonometric Functions	33
	Jacobi Elliptic Functions and Nested Lambert W	36
5.0.3	Some Special Cases	38
6	Conclusion	42
	Bibliography	43
	Curriculum Vitae	44

List of Figures

1.1	A handful of Taylor series approximations for the principal branch of the function $x^{\frac{1}{3}}$. To the right, the error function (1.3) is plotted for the same approximations. Note that the axes are uneven on the right. This was done to highlight error.	2
1.2	Taylor series approximations for each branch of $x^{\frac{1}{3}}$ as images of the domain curve $C = 2e^{it}$	2
1.3	Asymptotic approximations of the principal branch of W using (1.7). On the top, we fix $p = 0$ and vary N . On the bottom, we instead fix $N = 5$ and vary p . The graphs on their right are their respective forward error plots.	4
1.4	A plot of $ E_1 $ against $z = x + iy$. The plot shows that E_1 cannot be simplified to zero.	5
1.5	A plot of $ E_2 $ against $z = x + iy$. The plot shows that E_2 is zero everywhere in the complex plane. The random surface is the result of rounding errors.	6
2.1	The domains (left-hand axes) and ranges (right-hand axes) of the branches of the Lambert W function. The branches of W collectively fill all of the right-hand complex plane, although any one branch occupies only a disjoint strip of the plane. Each branch has a domain consisting of the entire complex plane, although the branch cuts differ according to the branch. The continuous curves in the range are constructed piecewise by mapping the circles successively with the different branches.	9
2.2	A comparison between the exact value of W and the one-term and two-term approximations in (2.6). The dashed curve is the exact value. The colours show where the branch boundaries are predicted to be by the approximations.	11
2.3	A systematic test of expansion (2.9), using two terms of the summation. Each continuous curve is a concatenation of mappings of the same large circle using successively the various branches of W and of its approximations. The dashed curves are the exact values of W_k while the solid curves are the approximations. The contours correspond to circles of radii, from right to left, $r = 50, 10, 5, 3, 1, e^{-1}$. The approximations to the principal branch for $r < 3$ are so bad that they distract from the plots and have been omitted. For non-principal branches, all approximations are plotted.	13

2.4	A comparison of possible asymptotic approximations to W_k for small circles around the origin. Two candidates are shown: $\ln_k z$ used for large circles and a new shifted logarithm. Note that $W_{-1}(x)$ and the shifted logarithm are both purely real (although not equal, alas) for the same range of arguments. For completeness, the map of the principal branch is also shown (in red) to emphasize that it does not participate in the asymptotic behaviour.	15
2.5	Plots of $W_{-1}(x)$ and approximations based on (2.9) together with (2.15). The solid red line shows W_{-1} , the dashed green line shows (2.9) for $N = 0$, while the blue dotted line shows $N = 3$	16
2.6	Comparison of W_k , $k \neq 0$ and (2.9) using (2.15). The series uses $N = 1$ in order to separate the function and the approximation. The boundary between $k = -1$ and $k = 1$ is the negative real axis both for the function and for the approximation.	16
3.1	At fixed values of x_0 in $W_0(x_0)$, error can be reduced to 0 for various p . However, optimal p values do not carry over for other values of x_0	19
3.2	The error plot $ W_0(z_0) - W_0^*(z_0) $ for fixed moduli $r = 1, 2$ and several values of the argument θ . Here, $N = 5$ and u 's expansion is (1.7).	19
3.3	Above, $W(x_0) - W_0^*(x_0)$ is plotted with respect to p for various values of x_0 using the same expansion of u as before. Here, $N = 15$. In the table below, Maple's RootOf command is used to find a zero close to $p = 4$ for the different values of x_0 and N	19
3.4	$W_0^*(x_0)$ plotted with two different zeroes of the error for $x_0 = 1$. Here, the values of p were found using $N = 10$ and (1.7) for u	20
3.5	Manual selection of intervals of θ where $W_0^*(re^{i\theta})$ diverges from W_0 . From top to bottom, $r = 3, 2$, and 1 , with $N = 70$ and $p = 0$ using (1.7).	21
3.6	Circles from 3.5 (along with others) plotted together, showcasing their intervals of divergence.	22
3.7	The circles from 3.6 put over a more complete region of divergence.	22
3.8	Domain coloring of the error of $W_0^*(z)$ using (1.7). From left to right, $\{N, p\} = \{5, 0\}, \{10, 0\}$, and $\{5, 3.066594076\}$	23
3.9	Domain coloring of the error for the 1 branch (left) and -1 branch (right). $\{N, p\} = \{5, 0\}$ in the top two plots and $\{5, 3.066594076\}$ in the bottom two. . . .	24
4.1	$\mathfrak{B} = \frac{1}{W(x)}$ plotted on the real axis. The two branches are colored with blue and red, respectively.	26
4.2	$y = \sin(x)e^{\sin(x)}$ compared with its inverse $\mathfrak{B}_0(x) = \arcsin_0(W_0(x))$. The principal branch's inverse is highlighted in blue on the left.	26
4.3	Branch structures for $\mathfrak{B} \in \mathfrak{L}$ over \mathbb{C} . $\mathfrak{B}_{[k,\ell]}(z) = \arcsin_\ell(W_k(z))$ is pictured on the left, $\mathfrak{B}_k(z) = \frac{1}{W_k(z)}$ on the right. On the left, arcsine branches are separated by dotted lines, and $W_k(z)$ branches are conversely distinguished by dashed lines.	28
5.1	Approximations of $\mathfrak{B}_0(x) = \frac{1}{W_0(x)}$ with independent variations of N and p using (1.7). On the left, $p = 0$ and on the right, $N = 10$	30

5.2	Approximations of images under $\mathfrak{B}_k(z) = \frac{1}{W_k(z)}$ using (1.10) and (2.15) with (1.7), respectively. On the left, $r = 4$. $r = 0.3$ on the right.	30
5.3	Approximations of $\mathfrak{B}_{\{k,\ell\}}(z)$ for the sine and cosine cases in \mathbb{C} , respectively. Here, the images are of a circle of radius $r = 1$ using the series (1.7).	31
5.4	Approximations of $\mathfrak{B}_{\{0,0,0\}}(z m) = F_{\{0,0\}}(W_0(x) m)$ for various values of the modulus m in \mathbb{C} . The images are of a circle of radius $r = 0.8$ using (1.7), with each approximation (in color) set against their respective expected image (in black).	32
5.5	Approximations of $\mathfrak{B}_{\{k,\ell\}} = W_\ell(W_k(z))$ over \mathbb{C} using images of a circle of radius $r = 1$ and the approximation (1.7).	32
5.6	A nested series approximation of $\mathfrak{B}_0(x) = \frac{1}{W_0(x)}$ for various numbers of terms M using (1.7) and (5.4). $N = 10$ and $p = 6$	34
5.7	The analog to figure 5.6 in \mathbb{C} , showing the divergence of the nested series for larger values of z	34
5.8	Real nested approximations of $\mathfrak{B}_{\{0,0\}}(0) = \arcsin_0(W_0(x))$ for different numbers of terms M . Here, we are using (1.7).	35
5.9	In \mathbb{C} , the prior approximation does not work as well outside of the principal branch.	36
5.10	On the real principal branch of $\mathfrak{B}(\varphi, \frac{1}{2}) = F_{\{\ell,j\}}(W_k(\varphi), \frac{1}{2})$, the nested series converges to the naive method for small A and B when using (1.7).	37
5.11	The images of a circle of radius $r = 1$ under the same nested series approximation of $\mathfrak{B}(z)$ in \mathbb{C}	38
5.12	Naive and nested series approximations of $\mathfrak{B}(x) = x$ on \mathbb{R} using (1.7).	39
5.13	Naive approximations of a circle of radius $r = 1$ using $\mathfrak{B}^*(z)$ and (1.7). Here, $N = 10$ and $p = 6$	40
5.14	Nested series approximation of z for various terms numbers M of the ze^z Taylor series, where $W_k^*(z)$ is using (1.7). $N = 10$, $p = 6$ and $k = 1$	40
5.15	Comparisons of approximations of the principal branch of $\mathfrak{B}_0 = e^{W_0(x)}$ over \mathbb{R} . On the right, the Taylor series approximation of $W_0(x)$ at $x = 0$ is used. Similarly, the right image uses the asymptotic approximation with (1.7). Here, $N = 10$ and $p = 6$	41

List of Tables

2.1	Numerical tests of convergence for the expansion (2.9). The row $N = \infty$ refers to the value of W that the series is trying to reach. The series appears convergent, although painfully slowly.	13
2.2	Comparison of series (2.9) combined with (2.7) and then with (2.15). The various approximations are printed in adjacent columns for easy comparison. The errors reported in the last two columns report the errors in the 4-term summations.	17
4.1	Riemann surfaces for different $\mathfrak{B}_k(z)$, with the branches colored separately to denote branch number from $k = -2$ to $k = 2$	27

Chapter 1

Introduction: Series Over Multivalued Functions

Multivalued functions defy the broadest definition of a mathematical function. Even at their most basic, we receive two or more outputs for some domain. Sidestepping this violation of a most elementary concept in mathematics can be done with a certain methodology - treating separate functions as interdependent components of a whole function. Treating intervals of the image as unique “branches”, the theoretical union of which being a complete inverse of a function, allows for more rigorous analysis.

1.1 Taylor Series for an Elementary Multifunction

An illuminating example of Taylor series arises from one of the most basic inverse functions. For the family of univariate power functions of the form $f(z) = z^n$, $z \in \mathbb{C}$, $n \in \mathbb{Z}$, the inverse function must be categorized into different branches. From here on, branches will be denoted with k unless noted otherwise. Letting $n = 2$, we obtain the near-trivial case of the square root function. Both branches are can be represented on the real plane, merely differentiated by the sign out front.

For $n \geq 2$, entire branches only appear in the complex plane. Every branch is thus separated by a factor of $e^{\frac{2ik\pi}{n}}$, $k \in \mathbb{Z}$. Though this is done by undergrads as an introductory exercise in complex analysis, it is still worth investigating as a multivalued function. And, as these are analytic functions on a disc in \mathbb{C} not including 0, they admit power series representations. For $n = 2$, the positive branch of $f(z)$ at z_0 has the following power series representation, given by Benghorbal in [20].

$$\sqrt{z} = \frac{\sqrt{\pi}}{2} \sum_{\ell=0}^{\infty} \frac{z_0^{\frac{1}{2}-\ell} (z - z_0)^\ell}{\Gamma(\frac{3}{2} - \ell)\ell!} \quad (1.1)$$

And with some work, this can be generalized to any value of $n \in \mathbb{N}$:

$$\sqrt[n]{z} = e^{\frac{2ik\pi}{n}} \sum_{\ell=0}^{\infty} \frac{\sqrt{\pi}}{2} \frac{z_0^{\frac{1}{n}-\ell} (z - z_0)^\ell}{\Gamma(1 + \frac{1}{n} - \ell)\ell!}, k \in \mathbb{Z} \quad (1.2)$$

Here, k is the branch number of the function we are attempting to approximate.

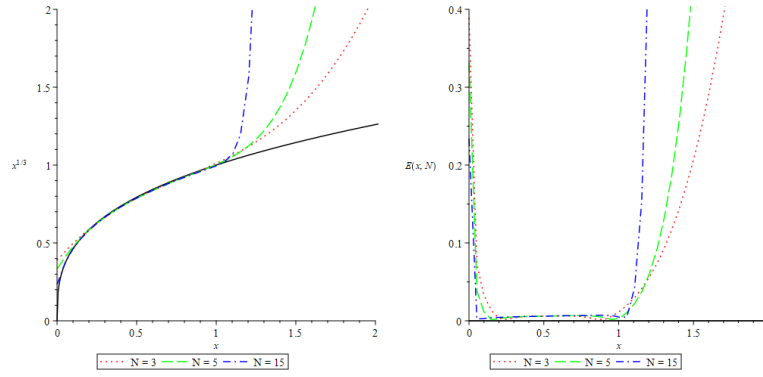


Figure 1.1: A handful of Taylor series approximations for the principal branch of the function $x^{\frac{1}{3}}$. To the right, the error function (1.3) is plotted for the same approximations. Note that the axes are uneven on the right. This was done to highlight error.

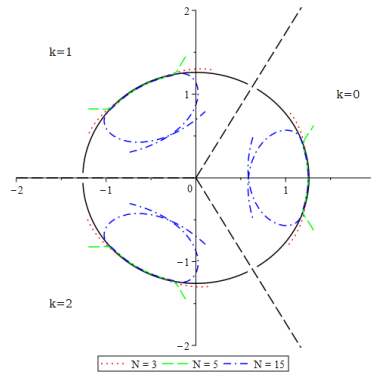


Figure 1.2: Taylor series approximations for each branch of $x^{\frac{1}{3}}$ as images of the domain curve $C = 2e^{it}$.

As an example, let $n = 3$ and $z_0 = \frac{1}{2}$. The real principal branch, $k = 0$, is plotted in Figure 1.1 and compared with various Taylor series approximations with different numbers of terms N . In addition, it is worth defining an error function $E(x)$ as follows:

$$E(z, N) = \left| \frac{\sqrt{\pi}}{2} \sum_{\ell=0}^N \frac{z_0^{\frac{1}{3}-\ell} (z - z_0)^\ell}{\Gamma(\frac{4}{3} - \ell)\ell!} - z^{\frac{1}{3}} \right| \quad (1.3)$$

Now, when plotting the other branches, another method is necessary. This is due to the four-dimensional nature of functions in \mathbb{C} , which can be captured by domain coloring. We may also use images of curves. By defining a curve C in the domain space, we can compare the images of C under both the function and its approximations. Setting $C = 2e^{it}$ and $k = 0, 1, 2$, we obtain a more complete picture of the accuracy of our previous Taylor series. Here, the branches are separated by dashed radial lines from the origin. Within each branch, the Taylor series approximations act the same, being accurate to the image under the cube root function.

Other elementary multivalued functions also have trivial connections between their branches. For example, $\arcsin(z)$ has branches defined as $(-1)^k \arcsin_0(z) + k\pi$, $k \in \mathbb{C}$, where $\arcsin_0(z)$ is the principal branch of arcsine. More important to our purposes later, the complex logarithm has

branches separated by a factor of $2ik\pi, k \in \mathbb{Z}$. To get approximations of these functions, one needs only to make respective adjustments to their series.

1.2 Series Approximations of The Lambert W Function in \mathbb{R}

All of the prior examples of multifunctions arise from inverting periodic elementary functions. The question of branches becomes more complicated once extra elements are added, even if said elements are not complicated themselves. In [1], the delay differential equation

$$\dot{y}(t) = ay(t - 1)$$

is solved with the inverse of the function $f(t) = te^t$, also known as the Lambert W function.

The Lambert W function's branches are not elementary in their relation with each other. Over \mathbb{R} , two branches exist, labeled as the principal branch and the -1 branch. A branch cut exist at $x = -\frac{1}{e}$, with the principal branch defined over the interval $[-\frac{1}{e}, \infty)$ and the -1 branch defined over $[-\frac{1}{e}, 0)$. As $x \rightarrow \infty$, the principle branch asymptotically approaches $\ln x$.

For the principal branch, a few well-known series are already defined. For example, the principal branch has a Taylor series with a radius of convergence of $\frac{1}{e}$ and is defined as follows:

$$W_0(x) = \sum_{n=1}^{\infty} (-n)^{(n-1)} \frac{x^n}{n!}, |x| < \frac{1}{e} \quad (1.4)$$

As this Taylor series is quite limited in its convergence, other series have been found that converge to W asymptotically. To receive these, start with an approximation $W_0(x) \approx \ln x + u$. Then, by plugging the approximation back in the original definition:

$$\begin{aligned} x(\ln x + u)e^u &= x \\ \implies u &= -\ln(\ln x) + v \\ \implies e^{-v} &= 1 - \frac{\ln(\ln x)}{\ln x} + \frac{v}{\ln x} \end{aligned}$$

After defining $\tau = \frac{\ln(\ln x)}{\ln x}$ and $\sigma = \frac{1}{\ln x}$, the above equation is known as the ‘‘fundamental relation’’.

$$e^{-v} - 1 + \tau - v\sigma = 0 \quad (1.5)$$

Utilizing Stirling numbers, Comtet [17] found a solution to this relation in the form of an asymptotic series. The numbers within the brackets represent Stirling cycle numbers. Furthermore, another expansion was found by Jeffrey [21] which utilizes Stirling 2-subset numbers. These asymptotic series are written as:

$$W_0(x) = \ln x - \ln(\ln x) + u \quad (1.6)$$

where u is, respectively,

$$\sum_{n=1}^{\infty} \sum_{m=1}^n \left[\begin{matrix} n \\ n-m+1 \end{matrix} \right] \frac{(-1)^{n-m} \sigma_k^{n-m} \tau_k^m}{m!} \quad (1.7)$$

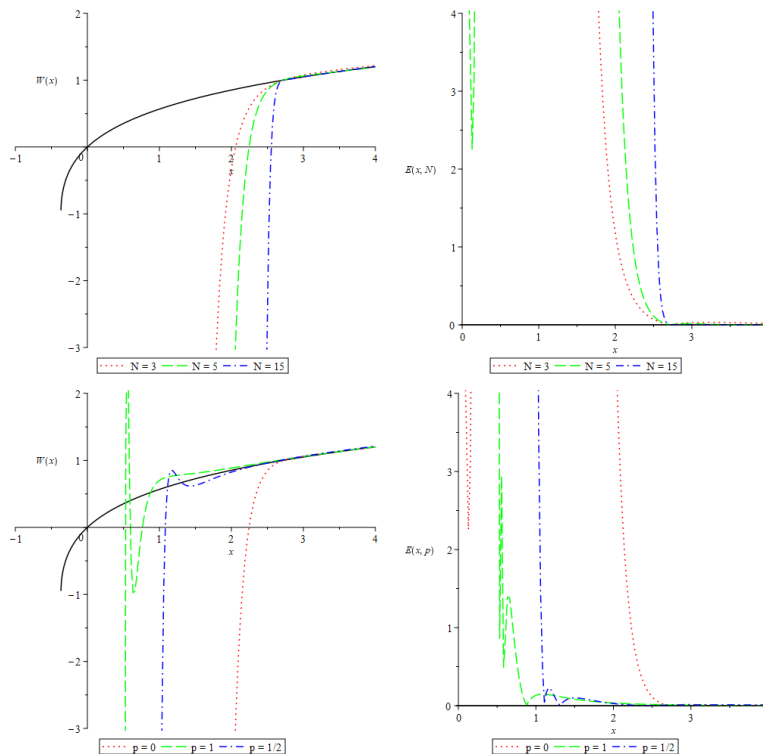


Figure 1.3: Asymptotic approximations of the principal branch of W using (1.7). On the top, we fix $p = 0$ and vary N . On the bottom, we instead fix $N = 5$ and vary p . The graphs on their right are their respective forward error plots.

$$\sum_{n=1}^{\infty} \sum_{m=0}^{n-1} \left\{ \begin{matrix} m+n-1 \\ m \end{matrix} \right\}_{\geq 2} \frac{\tau_k^n (-1)^{m+n-1}}{n!(1+\sigma_k)^{m+n}} \quad (1.8)$$

Additionally, define $u_{n,m}$ to be the n, m -th term of u . Both of these approximations will be integral to the following sections of the paper, as they can be generalized to any branch.

Shifting focus back to the principal branch for the moment, it is also worth mentioning a development found by Kalugin in [22]. The nested natural logarithm within the approximation of W_0 can be replaced by an "anstaz" $p + \ln x$, giving a new approximation

$$W_0(x) = \ln x - \ln(\ln x + p) + u \quad (1.9)$$

$$\sigma = \frac{1}{p + \ln x}, \tau = \frac{p + \ln(p + \ln x)}{p + \ln x}$$

This is possible due to (1.5) being invariant under this change. From here on, the term p will be referred to as a "p-correction", due to its effect on the asymptotic series. To show this quality, we compare the series at $p = 0$ with increasing values of N against various values of p for a fixed $N = 5$. Though the approximations at smaller values of x behave more erratically for a varying p , our series converge significantly earlier than by increasing N .

In [14], it was shown that these series could be generalized to any branch. This is due to the same property that allowed us to add the p -correction: invariance. Approximating $W_k(z) = \ln_k z + u$, where $\ln_k z = \ln_0 z + 2ki\pi, k \in \mathbb{Z}$, we get the same fundamental relation, albeit with

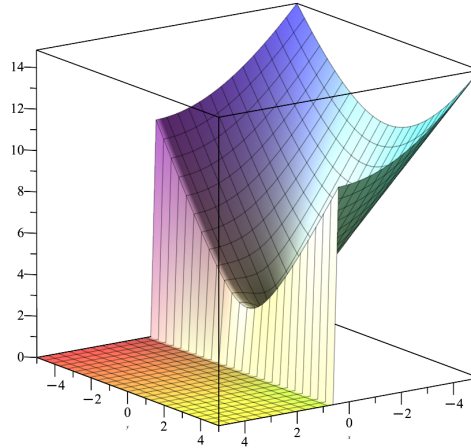


Figure 1.4: A plot of $|E_1|$ against $z = x + iy$. The plot shows that E_1 cannot be simplified to zero.

different definitions of τ and σ . With generalized component functions in our inventory, we receive an asymptotic series for any k^{th} -branch of the Lambert W function:

$$W_k(x) = \ln_k x + \ln_0(\ln_k x) + u \tag{1.10}$$

$$\sigma_k = \frac{1}{\ln_k x}, \tau_k = \frac{\ln_0(\ln_k x)}{\ln_k x}$$

1.3 W and multivalued functions in computer algebra

Research on Lambert W has significance for computer algebra systems beyond its own applications. Computer algebra systems have always had trouble manipulating and simplifying expressions containing multivalued functions. Early versions of Maple would simplify $\sqrt{-x} \rightarrow i\sqrt{x}$. Substituting $x = -1$ into this simplification resulted in $1 = -1$. Although this does not happen now, other problems persist. For example, consider the two expressions

$$E_1 = \sqrt{z+1} \sqrt{z-2} - \sqrt{(z+1)(z-2)}, \tag{1.11}$$

$$E_2 = \sqrt{1+z} \sqrt{2-z} - \sqrt{(1+z)(2-z)}. \tag{1.12}$$

One of these is zero everywhere in the complex plane, and one is not. Early versions of Maple would simplify both to zero, while current versions do not simplify either. We can discover graphically which it is by substituting $z = x + Iy$ into each expression and then plot $|E_1|$ and $|E_2|$ as a 3-D plot. The plots are shown in Figures 1.4 and 1.5.

A similar difficulty is seen in Maple's integration.

$$\int \frac{dz}{\sqrt{1+z} \sqrt{2-z}} = \frac{\sqrt{(1+z)(2-z)}}{\sqrt{1+z} \sqrt{2-z}} \arcsin(2z/3 - 1/3)$$

From the above discussion, the leading fraction is identically 1.

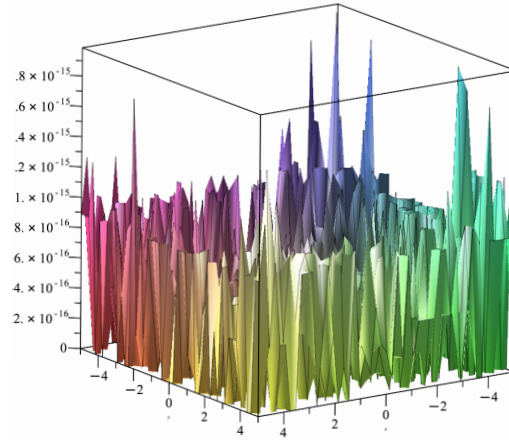


Figure 1.5: A plot of $|E_2|$ against $z = x + iy$. The plot shows that E_2 is zero everywhere in the complex plane. The random surface is the result of rounding errors.

A contributory blame for these problems is the unfocused thinking about multivalued functions in the literature. Working with the branches of W , we are forced to improve on this confusion. For example, the Digital Library of Mathematical Functions (DLMF) displays the following formulae (and, of course, many more)

$$\text{Log } z = \ln z + 2\pi i k, \quad (1.13)$$

$$\text{Arctan } z = \arctan z + k\pi, \quad (1.14)$$

$$\text{Arctan } u \pm \text{Arctan } v = \text{Arctan} \left(\frac{u \pm v}{1 \mp uv} \right). \quad (1.15)$$

We see that $\text{Log } z$ has a ‘hidden’ variable k , as does $\text{Arctan } z$. This implies that the equation (1.15) has 3 hidden variables. The equation betrays the attitude that branch selection can be postponed, or even relegated to a user and not a problem for the DLMF. This is not possible with W , because the branches are not trivially related, and decisions must be made at the time of definition and implementation. The first paper [1] used the $\text{Log } z$ notation, but quickly (the same year) [2] the notation

$$\ln_k z = \ln z + 2\pi i k$$

was proposed as a replacement. Although the proposal has not exactly gone viral, it will be used here.

Another way in which W is relevant to other studies is the shift in emphasis from the domain of the function to the range. It is in the range that branches are decided, rather than the domain. Influencers such as Kahan [3], however, focus entirely on branch cuts. The DLMF accompanies each definition of a multivalued function with a diagram of the branch cuts, but never with a diagram of the range. Further, the literature typically refers for a specific function to ‘the’ branch cut; here we show that each branch has different branch cuts and again simplistic approaches are inadequate.

We can note that Riemann surfaces are implicitly an acknowledgement that ranges are important, in that they layer range information over the function domain. Also the unwinding number can be regarded as a method to transfer range information back to the domain.

Chapter 2

Series for non-principal branches

2.1 Introduction

The Lambert W function owes its current status¹ in no small part to computer algebra systems, because they enabled the dissemination of information about W more widely than conventional publishing. Since W allowed algebra systems to return closed-form solutions to problems from all branches of science, users discovered W in ways that a literature search could not. Lambert W is multivalued, like arctangent or logarithm, and hence has branches. An important difference between the elementary multivalued functions and W is the fact that the branches of arctangent are trivially related, in that they differ by π ; similarly, the branches of logarithm differ by $2\pi i$. There is no simple relation between the branches of W , and each branch must be labelled separately and studied separately.

Definitions

The branches of the Lambert W function are denoted $W_k(z)$, where k is the branch index. Each branch obeys [1]

$$W_k(z)e^{W_k(z)} = z, \quad (2.1)$$

and the different branches are distinguished by the definition

$$W_k(z) \rightarrow \ln_k z \text{ for } |z| \rightarrow \infty. \quad (2.2)$$

Here, $\ln_k z$ denotes the k th branch of logarithm [2], i.e. $\ln_k z = \ln z + 2\pi i$, with $\ln z$ as defined in [4]. Definition (2.2) of the branches of W is also illustrated in Figure 2.1 below.

The principal branch $W_0(z)$ takes real values for $z \geq -e^{-1}$ and has been extensively studied. For example, the function $T(z) = -W_0(-z)$ is the exponential generating function for labelled rooted trees [5]; the convex analysis of W_0 was developed in [6]; in [7], it was shown that W_0 is a Bernstein function, and a Stieltjes function, and its derivative is completely monotonic; numerous papers have proposed numerical schemes for evaluating $W_0(x)$ for $x \in \mathbb{R}$, a recent example being [8]; a model of chemical kinetics in the human eye uses $W_0(x)$ in [9].

In contrast, *non-principal* branches $k \neq 0$ have been less studied, but nonetheless have applications. The branch $W_{-1}(z)$ takes real values for $-e^{-1} \leq z < 0$. The real-valued function

¹Citation counts as of July 2023: Google scholar 7278; Web of Science 4160.

$W_{-1}(-\exp(-1 - z^2/2))$ was used in [10] to obtain a new derivation of Stirling's approximation to $n!$ and Vinogradov has presented applications in statistics both for $W_{-1}(x)$ [11] and $W_0(x)$ [12].

2.2 Expansions

An important difference between W_0 and all other branches is behaviour at the origin. W_0 is analytic at the origin, and its Taylor expansion is known explicitly; in contrast, all other branches are singular at the origin. Our interest here is to study asymptotic expansions both for $|z| \rightarrow \infty$ and for $|z| \rightarrow 0$, of non-principal branches.

In [13], de Bruijn obtained an asymptotic expansion for $W_0(x)$ when $x \rightarrow \infty$; this was extended to the complex plane in [1], and to other branches in [14]. None of the papers attempted numerical tests of the series, neither for their accuracy, nor for exploring where the series are convergent and where purely asymptotic. This is the first aim here.

Further, having obtained an expansion for large x , [1] stated

A similar but purely real-valued series is useful for the branch $W_{-1}(x)$ for $x < 0$. We can get a real-valued asymptotic formula from the above by using $\log(-x)$ in place of $\text{Log}(z)$ and $\log(-\log(-x))$ in place of $\log(\text{Log}(z))$. [...] This series is not useful for complex x because the branch cuts of the series do not correspond to those of W .

We improve upon this point by proposing new, explicit series for all non-principal branches $k \neq 0$, and testing them numerically.

2.2.1 Branch structure

To focus our discussion, we consider the plots shown in Figure 2.1. The left-hand axes show values of z in the domain of $W(z)$. The right-hand axes show values of W_k , where the branch indicator k is important; that is, the right axes show the ranges² of W . Although only one set of axes is used to show the domain, this is a simplification which avoids multiple figures. There are actually several different domains, coinciding with the different branches of W . In contrast to more familiar multi-valued functions, such as $\ln z$, the different branches $W_k(z)$ do not share a single common domain. Specifically, the singular points and the branch cuts of $W_k(z)$ vary from branch to branch. In Figure 2.1, the different branch cuts for different branches are compressed onto the negative real axis (of the left set of axes) using the colours red and green. For the principal branch W_0 , the branch cut consists only of the red-coloured portion of the axis, i.e. $x \leq -1/e$, and the green segment is not a branch cut; the point $x = -1/e$ is the singular point. For the branches $k = \pm 1$, there are two branch cuts, coloured red and green; they meet at $x = -1/e$. It is best to think of the cuts as distinct, even though they share a singular point and also extend along the same axis. The distinction is that the red cut for $k = -1$ maps to the boundary between W_0 and W_{-1} , with the boundary belonging to W_{-1} , while the green cut maps to the boundary between W_1 and W_{-1} , with the boundary belonging to W_{-1} . Similarly, the red

²Note the plural. We regard each branch of W_k as a separate function with its own domain and range [15].

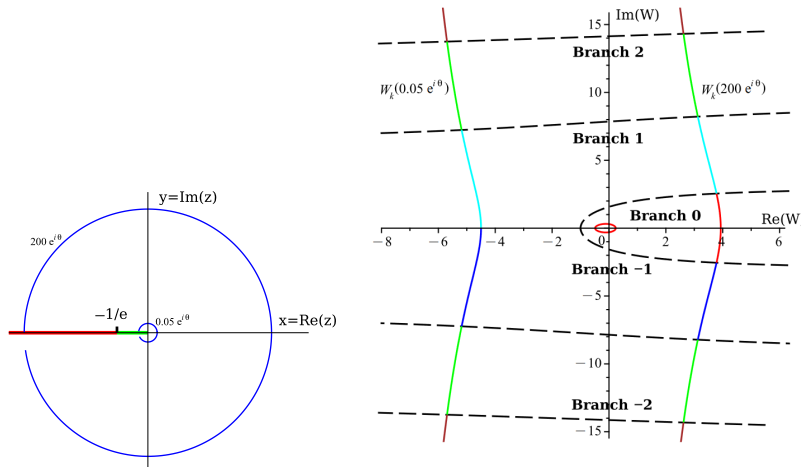


Figure 2.1: The domains (left-hand axes) and ranges (right-hand axes) of the branches of the Lambert W function. The branches of W collectively fill all of the right-hand complex plane, although any one branch occupies only a disjoint strip of the plane. Each branch has a domain consisting of the entire complex plane, although the branch cuts differ according to the branch. The continuous curves in the range are constructed piecewise by mapping the circles successively with the different branches.

cut for $k = 1$ maps to the boundary between W_0 and W_1 , but now the boundary belongs to W_0 . In contrast to the red cuts, the green cut maps to the boundary between W_1 and W_{-1} , with the boundary belonging to W_{-1} .

The origin is a second singular point for W_1 and W_{-1} . For all other branches, i.e. $k \geq 2$ and $k \leq -2$, the red and green cuts merge into a single cut extending along the whole of the negative real axis, with the point $z = -1/e$ no longer being a singular point, and only the origin being singular. Two circles, both alike in dignity³, are plotted in the domain; they are described by the equation $z = re^{i\theta}$ with $r = 200$ and $r = 0.05$ and $-\pi < \theta \leq \pi$. The circles are drawn so that one end of each circle touches the branch cut, while the other end stops short of the cut. This plotting convention reflects that the θ interval is closed on the top of the cut, when $\theta = \pi$.

The right-hand axes in Figure 2.1 show the ranges of the branches W_k . The branch boundaries are shown as black dashed lines. The curves plotted are the results from applying successively $W_{-2}, W_{-1}, W_0, W_1, W_2$ to the two circles shown in the left-hand axes. The colour-coded, but otherwise continuous, curve in the positive-real half-plane corresponds to the large circle, while the small circle maps into two curves: the small closed curve around the origin and the continuous curve in the negative real half-plane.

³This whimsical Shakespearian reference emphasises the mathematical point that previous investigations have concentrated on the large circle and neglected the equally important small circle.

2.2.2 Asymptotic expansions

We briefly summarize Poincaré's theory of asymptotic expansions [16, Ch.1]. We begin with an example.

$$\begin{aligned} g(x) &= \int_0^\infty \frac{e^{-xt} dt}{1+t} = \int_0^\infty e^{-xt}(1-t+t^2-t^3+\dots) dt \\ &= \frac{1}{x} - \frac{1!}{x^2} + \frac{2!}{x^3} - \frac{3!}{x^4} + \frac{4!}{x^5} - \dots \end{aligned} \quad (2.3)$$

The series in $1/x$ does not converge for any x , but if we substitute $x = 10$ into the equation, we obtain (evaluating the integral using Maple)

$$\int_0^\infty \frac{e^{-10t} dt}{1+t} = 0.0915633\dots = 0.1 - 0.01 + 0.002 - 0.0006 + 0.00024 - \dots \quad (2.4)$$

Adding the first 4 terms, we obtain the approximation 0.0914, which approximates the integral with an error 0.00016. Our sum omitted the 5th term, and we note that its value, 0.00024, bounds the observed error. It is typical of asymptotic series that the error is bounded by the first omitted term in the sum.

The theory of asymptotic expansions generalizes the functions x^{-k} used in the example, with a sequence of gauge, or scale, functions $\{\phi_n(x)\}$ obeying the condition $\phi_{n+1}(x) = o(\phi_n(x))$ as $x \rightarrow \infty$. The series formed from these functions,

$$g(x) = \sum_{n=1}^N a_n \phi_n(x), \quad (2.5)$$

has the property that it becomes more accurate as $x \rightarrow \infty$. Typically, the error is bounded by the omitted term $\phi_{N+1}(x)$. For an asymptotic expansion, the limit $N \rightarrow \infty$ is of less interest than the limit $x \rightarrow \infty$, and will not exist for a non-convergent expansion. This paper uses scale functions $\phi_n(z) = 1/\ln^n(z)$. In order for the functions to decrease with n , we require that $|\ln z| > 1$, which in turn requires $|z| > e$ or $|z| < e^{-1}$. Then they form an asymptotic sequence both in the limit $|z| \rightarrow \infty$ and $|z| \rightarrow 0$.

2.2.3 Outline

In section 2.3, we revisit the derivation of the expansion of W given in [1] for large arguments, replacing the imprecise notation Log with the precise notation $\ln_k z$ defined above. We then use graphical methods to add to earlier treatments by demonstrating the accuracy of the approximations for the different branches. Although not all asymptotic expansions are convergent series, the expansions given here are convergent for some arguments. We show this convergence, but do not analyse the regions in detail.

In section 2.4, the main motivation for this paper is taken up: the expansions for non-principal branches of W around the origin. We show that the key idea is to define a shifted logarithm which matches the asymptotic behaviour at the origin. Again we also consider convergence, and we uncover an unexpected result that several series, although based on different starting assumptions, none the less converge to correct values. The rates of convergence, however, are different, with the series based on shifted logarithms being best.

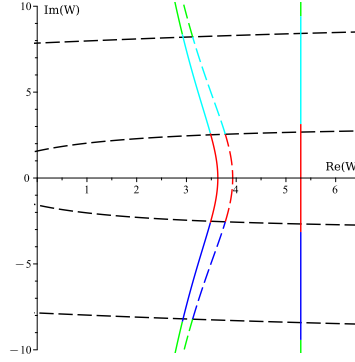


Figure 2.2: A comparison between the exact value of W and the one-term and two-term approximations in (2.6). The dashed curve is the exact value. The colours show where the branch boundaries are predicted to be by the approximations.

2.3 de Bruijn series for large z

Since the branches of W are defined so that $W_k(z)$ asymptotically approaches $\ln_k z$, we consider $W_k(z) = \ln_k z + v(z)$, and assume $v = o(\ln_k z)$. Then (2.1) gives

$$(\ln_k z + v(z)) e^{\ln_k z + v} = (\ln_k z + v(z)) z e^v = z .$$

To leading order, $e^{-v} = \ln_k z$, and assuming that v lies in the principal branch of logarithm, the approximation is (note the different branches of logarithm)

$$W_k(z) = \ln_k z - \ln_0(\ln_k z) + u(z) . \quad (2.6)$$

Neglecting temporarily the $u(z)$ term, we compare in Figure 2.2 the one-term and two-term approximations to W . The colour coding shows where the approximations think the branch boundaries are. The term $\ln_k z$ alone is a significant over-estimate, and the branch boundaries are not close, but two terms, although under-estimating, are encouragingly closer. Our main interest, however, is the behaviour after including $u(z)$. Substituting (2.6) into (2.1) and introducing

$$\sigma = \frac{1}{\ln_k z} , \quad \text{and} \quad \tau = \frac{\ln(\ln_k z)}{\ln_k z} , \quad (2.7)$$

we can show that u obeys (more details of this demonstration are given below)

$$1 - \tau + \sigma u - e^{-u} = 0 . \quad (2.8)$$

Equation (2.8) was solved for u by Comtet [17] as a series in σ :

$$u = \sum_{n=1}^N c_n \frac{(-\sigma)^n}{n!} , \quad (2.9)$$

$$c_n = \sum_{m=1}^n (-1)^{n-m} \left[\begin{matrix} n \\ n-m+1 \end{matrix} \right] \frac{\sigma^{-m} \tau^m}{m!} , \quad (2.10)$$

where $\left[\begin{smallmatrix} n \\ n-m+1 \end{smallmatrix} \right]$ is a Stirling Cycle number [18, p. 259], and we have written the series going to N terms, for later reference. The form of the expansion appears to be unchanged from the principal branch, but this is because the branch information is hidden in the variables σ and τ . The derivation of the expansion is for an asymptotic series, as defined in §2.2.2. Such series are not necessarily convergent⁴, but in [21], the series (2.6) together with (2.9) was studied for $x \in \mathbb{R}$ and the series was shown to converge for $x > e$. The question naturally arises of where the series for principal and non-principal branches converge for $z \in \mathbb{C}$.

Since we are dealing with the accuracy and convergence of series on multiple domains of z and for multiple branches of W , we wish to avoid analyzing each branch separately and being tempted to present multiple repetitious plots of results. We thus use the plot shown in Figure 2.3 to summarize our findings. The plot accumulates maps of the large circle shown above in Figure 2.1 under successive branches W_k ; these plots are compared with maps made by the corresponding series approximation (2.9) using 2 terms of the summation. The contours correspond to circles of radii $r = 50, 10, 5, 3, 1, e^{-1}$. In each case the dashed curve is W and the solid curve is the series approximation.

In Figure 2.3, we focus first on the approximation for the principal branch, indicated by the red curves. We see that for $r > 3$, the accuracy is acceptable, and improves for larger r , as expected. Since we are considering an asymptotic approximation, we fix the number of terms in the summation to 2, and consider changes with r . We note in particular that the exact and approximate curves for $r = 50$ are practically indistinguishable to the human eye. We can also investigate the convergence of the series. For $r > 10$ we can take more terms of the summation and observe improved accuracy (data not shown), indicating the series is convergent for larger r values (as well as asymptotic). For smaller values of r , the series loses accuracy, and in parallel fails to converge, the extraneous curves swamping the figure. Therefore, for $r < 3$ we plot only the values of W_0 and remove the distraction of the failed approximations.

Both the W curves and the approximations are smooth across the branch boundaries. This reflects the properties that

$$W_k(-x) = \lim_{y \uparrow 0} W_{k+1}(-x + iy), \quad \text{for } x < -1/e, \text{ and} \quad (2.11)$$

$$\ln_k(-x) = \lim_{y \uparrow 0} \ln_{k+1}(-x + iy), \quad \text{for } x < 0. \quad (2.12)$$

This does not ensure that the boundaries between the branches of W and of the approximations agree, although they approach each other with improved accuracy.

For branches $k \neq 0$, we observe something that is unexpected, namely, that the approximations show evidence of remaining accurate for all values of r down to $r = e^{-1}$. Indeed, the series appear convergent. This is difficult to justify graphically, but can be checked by extended summation for values where graphical evidence is weakest. In Table 2.1 we calculate approximations to $W_{-1}(-1/e) = -1$ and $W_{-1}(-0.4)$ using increasing numbers of terms in the sum. Adding up large numbers of terms in a sum can require additional intermediate precision for accuracy. For the table, Maple's default 10-digit accuracy had to be increased to 30 decimal digits for sums of more than 50 terms. The numerical results indicate convergence, but do not constitute a proof.

⁴Indeed, some authors define an asymptotic series as one that does not converge [19].

N	value for $x = -e^{-1}$	value for $x = -0.4$
∞	-1	$-0.9441 - 0.4073 i$
40	$-1.1568 - 0.1565 i$	$-0.9665 - 0.3495 i$
70	$-1.1190 - 0.1188 i$	$-0.9259 - 0.3800 i$
100	$-1.0997 - 0.0996 i$	$-0.9232 - 0.4055 i$
160	$-1.0789 - 0.0788 i$	$-0.9448 - 0.4183 i$

Table 2.1: Numerical tests of convergence for the expansion (2.9). The row $N = \infty$ refers to the value of W that the series is trying to reach. The series appears convergent, although painfully slowly.

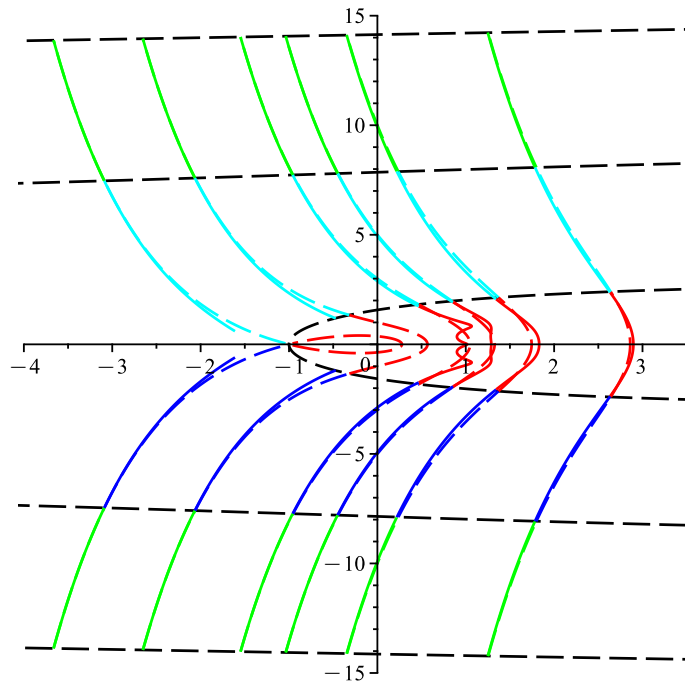


Figure 2.3: A systematic test of expansion (2.9), using two terms of the summation. Each continuous curve is a concatenation of mappings of the same large circle using successively the various branches of W and of its approximations. The dashed curves are the exact values of W_k while the solid curves are the approximations. The contours correspond to circles of radii, from right to left, $r = 50, 10, 5, 3, 1, e^{-1}$. The approximations to the principal branch for $r < 3$ are so bad that they distract from the plots and have been omitted. For non-principal branches, all approximations are plotted.

2.4 de Bruijn series for small z

A new feature associated with the analysis around the origin is the disappearance from the asymptotic analysis of the principal branch. Figure 2.4 shows a plot of values of W_k computed on a circle of radius $r = \frac{1}{20}$ and centred at the origin. The principal branch, shown in red, is the small closed curve around the origin, while all other branches form the continuous curve on the far left. It is important to note a difference between W_0 and W_{-1} . The real values of W_0 occur in the middle of its range, or to put it another way, the real values of W_0 do not coincide with the branch boundaries. In contrast, the real values of W_{-1} occur on one of its branch boundaries. We want this difference to be reflected, if possible, in the asymptotic forms we use. As in the previous section, the leading asymptotic term is logarithm, and the problem is to match the branches of the logarithm term to W_{-1} , and more generally to all W_k for $k \neq 0$. Two possible asymptotic approximations are shown in Figure 2.4 as the vertical lines to the right of the curve showing the values of W . The right-most line is the approximation $\ln_k z$ which was already used for the previous section. Since $W_{-1}(-0.01) = -6.473$, i.e. purely real, but $\ln(-0.01) = -4.605 + \pi i$ and $\ln_{-1}(-0.01) = -4.605 - \pi i$, it is clear that the approximations that worked well in the previous section, do not work here. For this reason, we introduce what we call a ‘shifted log’ by the definition

$$L_k(z) = \ln_k z - \operatorname{sgn}(k)i\pi, \quad \text{for } k \neq 0. \quad (2.13)$$

We see that for this function $L_{-1}(-0.01) = -4.605$, and so is purely real where W_{-1} is real. This function is plotted in Figure 2.4 as the straight line in between the other two contours. Notice that $W_{-1}(-e^{-1}) = -1$, and $L_{-1}(-e^{-1}) = -1$ also. Of course, $W_{-1}(z)$ is not differentiable at $z = -e^{-1}$, but $L_{-1}(z)$ is differentiable, showing that more terms in the series will be needed for numerical accuracy.

Having matched the leading-order behaviour of W_k using the shifted logarithm, we repeat the approach used above of substituting into $W e^W = z$.

$$\begin{aligned} (L_k(z) + v(z)) \exp(L_k(z) + v(z)) &= (L_k(z) + v(z)) (-z) \exp(v(z)) = z \\ v(z) &= -\ln(-L_k(z)) + u(z). \end{aligned}$$

It might seem that u will follow a pattern like $\ln(\ln(-L_k))$, but this is not so.

$$\begin{aligned} (L_k(z) - \ln(-L_k(z)) + u) \exp(L_k(z) - \ln(-L_k(z)) + u) \\ = (L_k(z) - \ln(-L_k(z)) + u) \frac{-z}{-L_k(z)} \exp(u) = z. \end{aligned}$$

Rearranging gives

$$1 - \frac{\ln(-L_k(z))}{L_k(z)} + \frac{u}{L_k(z)} - e^{-u} = 0. \quad (2.14)$$

Thus, if we redefine σ, τ by

$$\sigma = \frac{1}{L_k(z)} \quad \text{and} \quad \tau = \frac{\ln(-L_k(z))}{L_k(z)}, \quad (2.15)$$

we can return to (2.8) and (2.9).

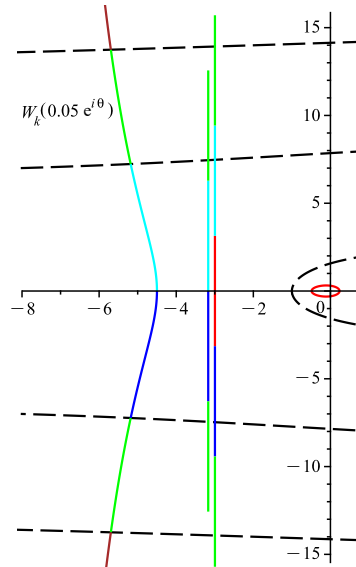


Figure 2.4: A comparison of possible asymptotic approximations to W_k for small circles around the origin. Two candidates are shown: $\ln z$ used for large circles and a new shifted logarithm. Note that $W_{-1}(x)$ and the shifted logarithm are both purely real (although not equal, alas) for the same range of arguments. For completeness, the map of the principal branch is also shown (in red) to emphasize that it does not participate in the asymptotic behaviour.

It is remarkable that the fundamental relation (2.8), originally derived for the principal branch, has now reappeared twice: once for any branch ($|z| \gg 1$) and now for $|z| \ll e^{-1}$. Since (2.13) was chosen so that it is purely real where W_{-1} is real, we first compare plots for $-e^{-1} \leq x < 0$. Figure 2.5 compares $W_{-1}(x)$ with two approximations, sum 2.9 for $N = 0$ and for $N = 3$. They are most accurate near $x = 0$ as expected.

Figure 2.6 shows a comparison in the complex plane for branches from $k = -2$ to $k = 2$. The contours are maps of small circles of radii $r = 0.15, 0.05$. The series approximation was limited to $N = 1$ in order to obtain a visible separation of the exact and approximate contours. Recall that smaller values of r correspond to contours further to the left.

2.5 A surprising convergence

The approximation (2.7) used for $|z| \gg 1$ was discarded for $|z| \ll -e^{-1}$ because the branch boundaries were not aligned with the function near negative infinity. One could expect therefore that its accuracy would be bad, or wrong, or it would possibly return values for branches not requested. It is therefore surprising that in spite of starting from dismal estimates, the approximation manages to achieve results of reasonable accuracy. In Table 2.2, a comparison is made between series (2.9) based on (2.15) with the rejected series based on (2.7). Out of curiosity, we have tabulated the competing approximations when summed to one-term, two-terms and four-terms. The preferred series always performs better, but the other series also achieves good accuracy. As stated several times, (2.15) has the advantage of returning real values when

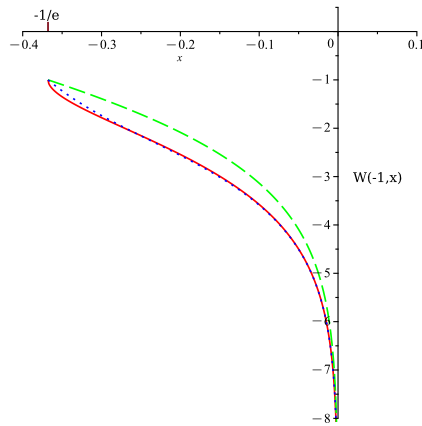


Figure 2.5: Plots of $W_{-1}(x)$ and approximations based on (2.9) together with (2.15). The solid red line shows W_{-1} , the dashed green line shows (2.9) for $N = 0$, while the blue dotted line shows $N = 3$.

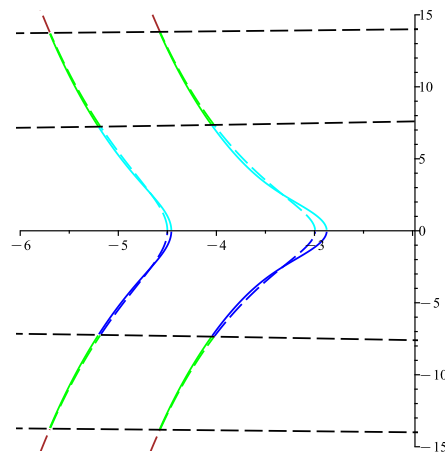


Figure 2.6: Comparison of W_k , $k \neq 0$ and (2.9) using (2.15). The series uses $N = 1$ in order to separate the function and the approximation. The boundary between $k = -1$ and $k = 1$ is the negative real axis both for the function and for the approximation.

x	k	W_k	$\ln_k x$	$L_k(x)$	Eq (2.7) $N = 0$	Eq (2.15) $N = 0$
-0.1	-1	-3.58	$-2.30 - \pi i$	-2.30	$-3.66 - 0.94i$	-3.15
-0.01	-1	-6.47	$-4.61 - \pi i$	-4.61	$-6.32 - 0.60i$	-6.13
-0.1	-2	$-4.45 - 7.31i$	$-2.30 - 3\pi i$	$-2.30 - 2\pi i$	$-4.58 - 7.61i$	$-4.20 - 7.50i$
-0.01	-2	$-6.90 - 7.08i$	$-4.61 - 3\pi i$	$-4.61 - 2\pi i$	$-6.96 - 7.40i$	$-6.66 - 7.22i$

x	k	W_k	Eq (2.7) $N = 2$	Eq (2.15) $N = 2$	Error (2.7)	Error (2.15)
-0.1	-1	-3.577	$-3.405 - 0.127i$	-3.591	0.213	0.013
-0.01	-1	-6.473	$-6.416 + 0.035i$	-6.481	0.066	0.008
-0.1	-2	$-4.449 - 7.307i$	$-4.448 - 7.314i$	$-4.442 - 7.305i$	0.0074	0.0071
-0.01	-2	$-6.896 - 7.081i$	$-6.891 - 7.086i$	$-6.894 - 7.079i$	0.0069	0.0039

Table 2.2: Comparison of series (2.9) combined with (2.7) and then with (2.15). The various approximations are printed in adjacent columns for easy comparison. The errors reported in the last two columns report the errors in the 4-term summations.

W_{-1} is real, so we stick to our preferred series and do not pursue further discussion of this point.

Chapter 3

Further Notes on Convergence

Though chapter 2 focuses on convergence of asymptotic expansions for non-principal branches of $W_k(z)$, some considerations were left out. For example, there are now two variants of the series for each expansion of u , but shared components of both have yet to be optimized. Furthermore, only images of curves in \mathbb{C} have been utilized rather than the whole complex plane. This chapter will focus on exploring these questions to assist with future computations.

3.1 Optimizing Asymptotic Approximations

In the previous two chapters, the parameter p was introduced as an invariant transformation which alters the convergence properties of $W_k^*(z)$. Here, $W_k^*(z)$ represents a general asymptotic expansion of $W_k(z)$. This parameter allows for an extended region of convergence, but we are lacking a thorough look into how p can be utilized more effectively. Thus, this section will investigate how much p can improve a series, allowing for lower numbers of terms and improved accuracy.

As will become custom in later sections, an appropriate place to start is the principal branch of $W(x)$ in \mathbb{R} . Utilizing expansion (1.7) in $W_0^*(x)$, we end up with several values of p which reduce the error to zero at fixed values $x_0 \in \mathbb{R}$. As shown in 3.1, plotting $|W_0(x_0) - W_0^*(x_0)|$ for different term values N reveals the oscillatory nature of the error. Each plot crosses the p -axis several times, and each choice of N has a separate set of zeroes.

Figure 3.1 highlights that distinct choices of x_0 determine the set of error-minimizing p values as well. Moving over to \mathbb{C} presents an abstraction of this issue, as values of z_0 with the same modulus but different arguments θ will have different errors. Over the complex principal branch, plotting the error $|W_0(z_0) - W_0^*(z_0)|$ in figure 3.2 shows that p cannot reduce the error to 0 for all θ . In fact, the question of finding the objectively best value of p would require p to be redefined as a function of z_0 and N rather than a constant.

This itself is a dubious task, as there are several values of p which minimize the error for any given z_0 . Instead, a more efficient method is to find a constant p which reduces N while also keeping error low for values of z surrounding z_0 . Special attention must be given to the behaviour of the error around each zero, as more erratic behaviour spells out less stable convergence. Figure 3.3 shows that, for the real principal branch $W_0(x)$, more “stable” zeros of $W(x) - W_0^*(x)$ occur later as the error varies wildly for smaller values of p . Plotting $W_0^*(x)$ again

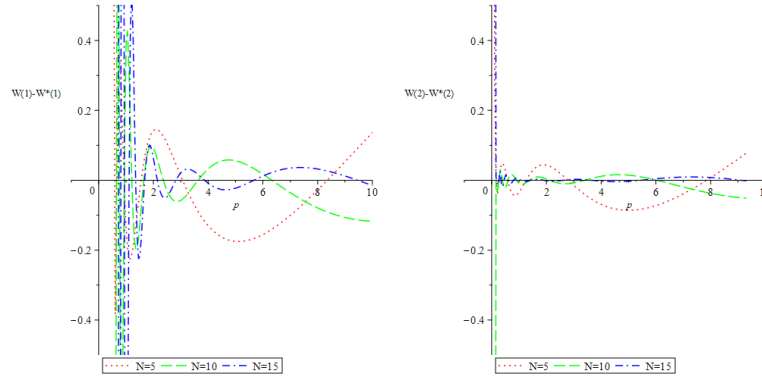


Figure 3.1: At fixed values of x_0 in $W_0(x_0)$, error can be reduced to 0 for various p . However, optimal p values do not carry over for other values of x_0 .

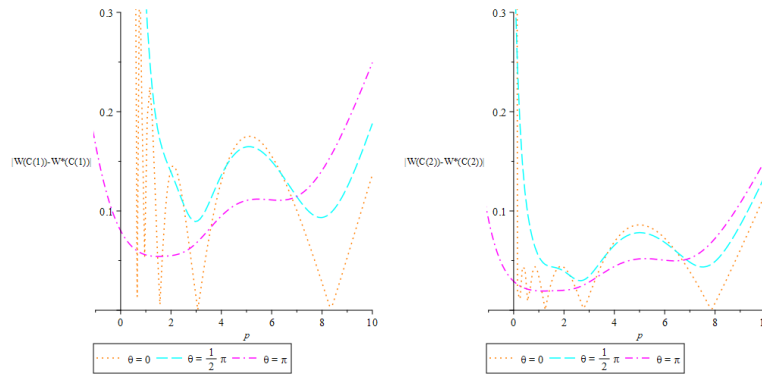
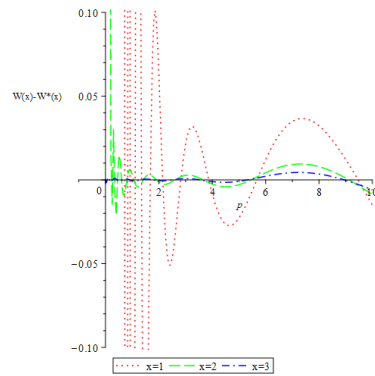


Figure 3.2: The error plot $|W_0(z_0) - W_0^*(z_0)|$ for fixed moduli $r = 1, 2$ and several values of the argument θ . Here, $N = 5$ and u 's expansion is (1.7).



	N=5	N=10	N=15
x = 1	3.066594076	3.632618669	3.870615051
x = 2	2.790452350	3.400177010	3.663439218

Figure 3.3: Above, $W(x_0) - W_0^*(x_0)$ is plotted with respect to p for various values of x_0 using the same expansion of u as before. Here, $N = 15$. In the table below, Maple's RootOf command is used to find a zero close to $p = 4$ for the different values of x_0 and N .

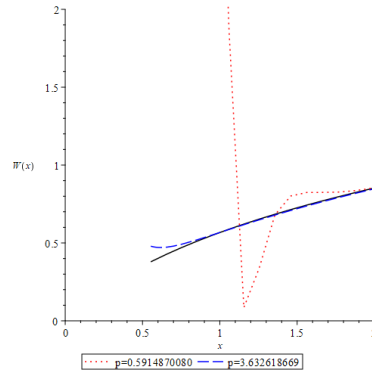


Figure 3.4: $W_0^*(x_0)$ plotted with two different zeroes of the error for $x_0 = 1$. Here, the values of p were found using $N = 10$ and (1.7) for u .

with the values of p found in 3.3 shows greatly improved convergence, especially compared to a more unstable zero.

3.2 Convergence Over the Complex Plane

Previously, when testing the accuracy of $W_k^*(z)$ in \mathbb{C} , we had only utilized images of circles in complex space. Though this does provide a relatively low-storage method of studying the properties of our prior series, there is something crucial left out of our discussion. Namely, we are left without a generalized view of \mathbb{C} as a whole. To build up to a more complete picture, start by utilizing properties of the circles from chapter 2.

By taking a circle $re^{i\theta}$, we may vary the radius for moderately small values, say $1 < r < 4$. Letting $p = 0$ and N be large in our thought experiment, we want to find the intervals of θ for which the approximations lose convergence. The principal branch will be a suitable starting point for this investigation, as decreasing z will cause the loss of convergence there earlier than non-principal branches. Furthermore, the approximations are symmetric about the real axis. This hints at a region of instability which carries a symmetrical shape.

Starting with a large radius of $r = 3$ with $N = 70$ in figure 3.5, we manually record the values of θ for which $W_0^*(re^{i\theta})$ loses convergence. Decreasing the radius shows that the region which $W_0^*(x)$ diverges expands as r becomes smaller. Between $r = 2$ and $r = 1$, the two divergent intervals of θ combine into a single interval. A collage of all the circles $re^{i\theta}$ is plotted in figure 3.6.

Though this works fine at establishing a general shape of the region of divergence, it must be noted that the previous task was done by brute force. Each circle required some trial-and-error to find its appropriate intervals. Thus, one may be compelled to find a more rigorous way to plot the region. This can be done via domain coloring, where the function is defined as $|W_k(z) - W_k^*(z)|$. We will use this function on its own later, but by additionally recording the last value of the difference within a tolerance after several iterations, we get a cleaner picture of the region of divergence. This is shown in figure 3.7, where black and white regions are the most divergent.

Now that a region of divergence has been established, it is appropriate to look at the raw

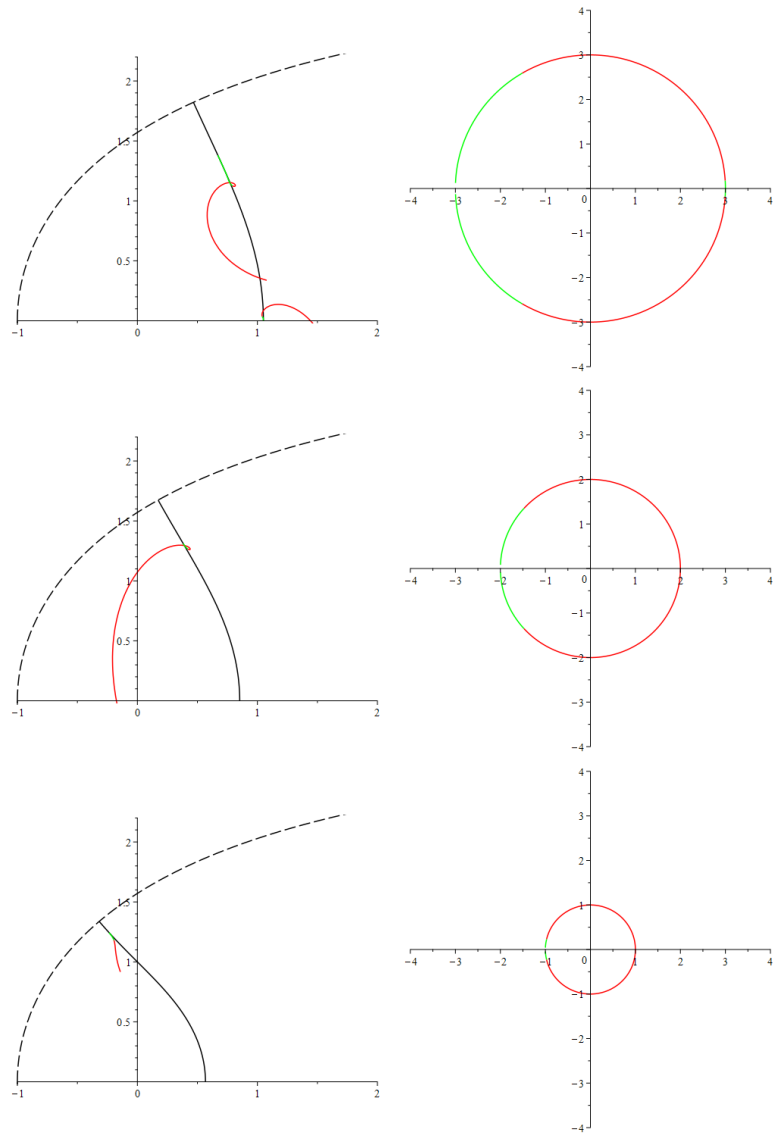


Figure 3.5: Manual selection of intervals of θ where $W_0^*(re^{i\theta})$ diverges from W_0 . From top to bottom, $r = 3, 2$, and 1 , with $N = 70$ and $p = 0$ using (1.7).

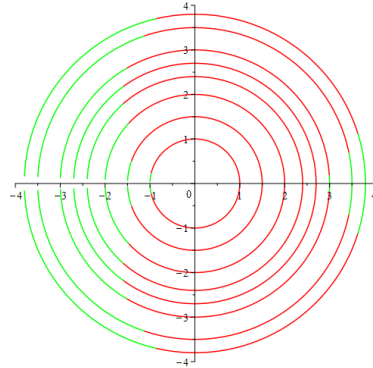


Figure 3.6: Circles from 3.5 (along with others) plotted together, showcasing their intervals of divergence.

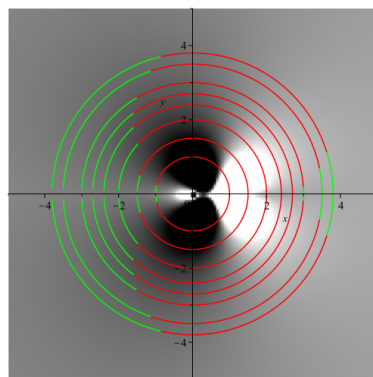


Figure 3.7: The circles from 3.6 put over a more complete region of divergence.

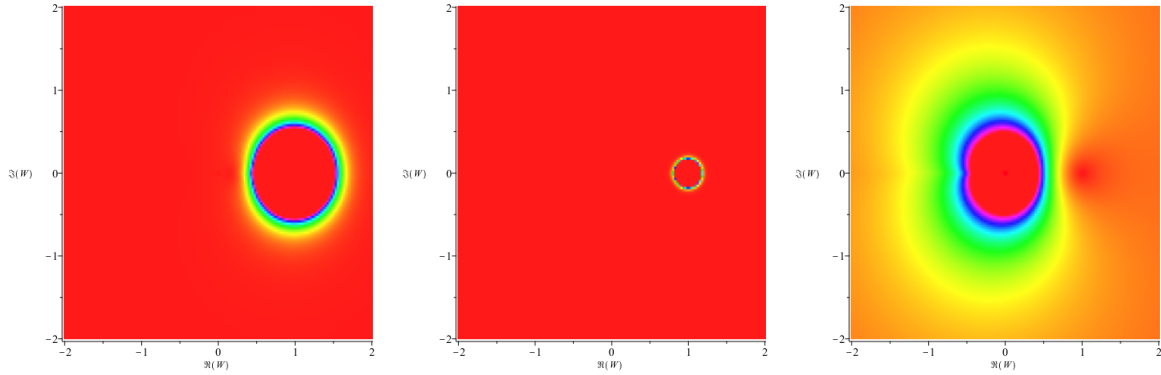


Figure 3.8: Domain coloring of the error of $W_0^*(z)$ using (1.7). From left to right, $\{N, p\} = \{5, 0\}, \{10, 0\}$, and $\{5, 3.066594076\}$.

behaviour of the error over \mathbb{C} . In the prior example, the error was constrained by a tolerance. Now we ignore that tolerance. Two ways of imaging the accuracy of $W_k^*(z)$ for all of $z \in \mathbb{C}$ are as follows: plot Riemann surfaces, or do more domain coloring. Though Riemann surfaces may look more impressive, the visual clutter of two surfaces make domain coloring the better option.

To do the domain coloring, return to the initial definition of the error function: $|W_k(z) - W_k^*(z)|$. Starting with the complex principal branch, the values of z where $W_k^*(z)$ diverges lie in a circular region to the right of the origin. Setting $p = 0$ and increasing N reduces the size of this region. In figure 3.8, the convergent regions are represented by warm colors. Conversely, $W_k^*(z)$ diverges for values of z in the cool-coloured region. Referring back to figure 3.3, using the value of p for $x = 1$ and $N = 5$ now results in a drastically altered plot. Though the convergent region accommodates smaller values on the positive real axis, more of the complex plane diverges around the origin.

Imaging the -1 and 1 branches reveals drastically different divergent regions of \mathbb{C} . Whereas the divergent region of the principal branch is symmetric over the positive real axis, the divergent regions of the 1 and -1 branches are semicircular. Furthermore, both regions are reflected versions of each other over the real axis. Adding values of p from 3.3 has an effect similar to the principal branch; smaller values on the positive real axis now converge at the cost of a larger divergent region.

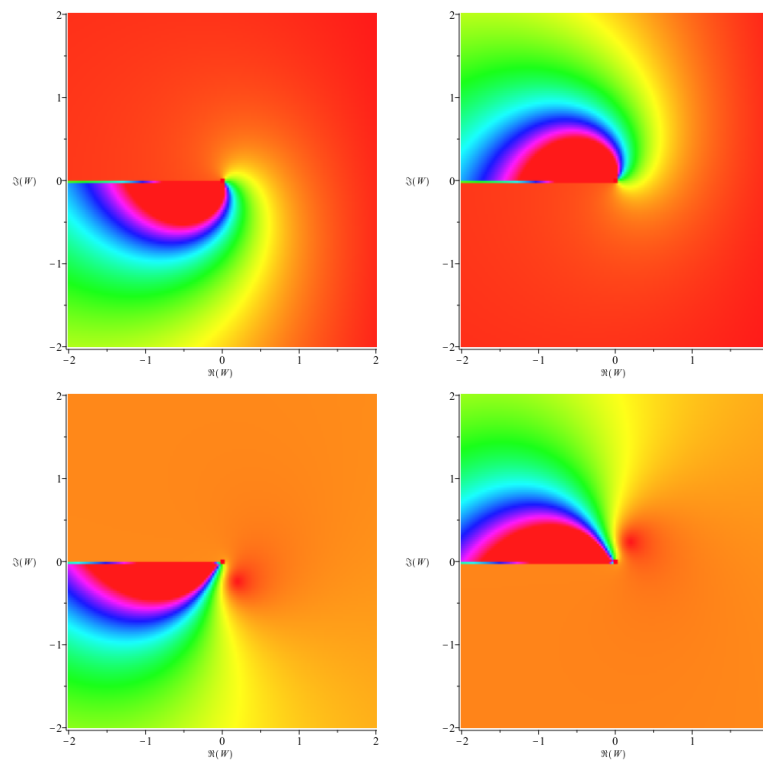


Figure 3.9: Domain coloring of the error for the 1 branch (left) and -1 branch (right). $\{N, p\} = \{5, 0\}$ in the top two plots and $\{5, 3.066594076\}$ in the bottom two.

Chapter 4

A Family of Functions Related to Lambert W

Compared with other well-known non-elementary multifunctions, the Lambert W function has rather interesting behaviour over all of its branches. As shown previously, the manner in which each branch is connected is non-trivial. Other well-studied special functions have rather elementary connections between branches. For example, take the Jacobi elliptic functions. $\operatorname{sn} z$ and $\operatorname{cn} z$ are doubly periodic, and their multivalued inverses consequently have branches separated by a factor of either period.

When attempting to find any other multivalued function which has non-trivial connections between branches, it is worth looking back to functions related to W itself. The second approximation (1.8) found in [21] arose from the study of the inverse functions of $x^\alpha e^x$, and this can be taken even further. A curious side-effect of the fundamental relation and its malleblility is that it extends to a family of functions related to W . To get to these results, we must first establish some analytical properties of these functions.

4.1 Analysis of Select Functions

Say we have some function $g(x)$ over \mathbb{R} . Through composition with the function $f(x) = xe^x$, we obtain a family of functions of the form $g(x)e^{g(x)}$. Similar to the Lambert W function is the resulting class of inverse functions. These are of the form

$$\mathfrak{B}(x)e^{\mathfrak{B}(x)}$$

where $\mathfrak{B}(x) = (g^{-1} \circ W)(x)$. Let this family of functions be denoted by \mathfrak{Q} , where each \mathfrak{B} is a member. This family of functions has rather fascinating members, and it is worth starting our analysis with specific cases. For example, set $g(x) = \frac{1}{x}$. In this case, $\mathfrak{B}(x) = \frac{1}{W(x)}$.

On \mathbb{R} , this function has a branch cut at $x = -\frac{1}{e}$. The two branches are defined in a fashion quite different to W . The -1 branch is defined over the interval $[-\frac{1}{e}, 0)$, and its range only covers the interval $[-1, 0]$. Conversely, the principal branch, $\mathfrak{B}_0(x) = \frac{1}{W_0(x)}$, is defined over the interval $[-\frac{1}{e}, 0) \cup (0, \infty)$. The asymptotic behaviour has also changed relative to the Lambert W function. Rather than converging to $\ln x$ as $x \rightarrow \infty$, we instead have a principal branch which

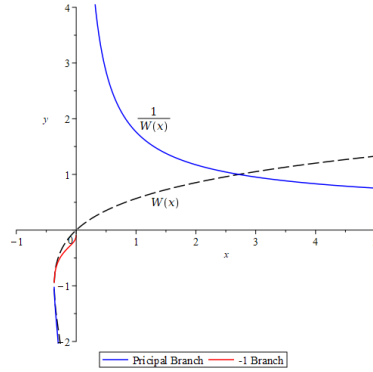


Figure 4.1: $\mathfrak{B} = \frac{1}{W(x)}$ plotted on the real axis. The two branches are colored with blue and red, respectively.

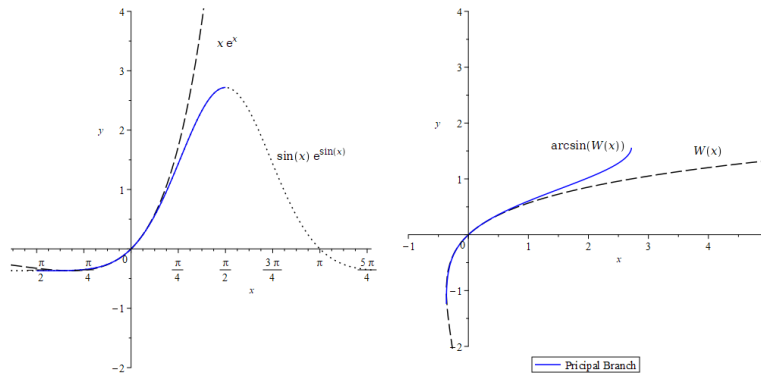


Figure 4.2: $y = \sin(x)e^{\sin(x)}$ compared with its inverse $\mathfrak{B}_0(x) = \arcsin_0(W_0(x))$. The principal branch's inverse is highlighted in blue on the left.

is bounded below by $\frac{1}{\ln x}$ as $x \rightarrow \infty$. The only place which this choice of $\mathfrak{B}(x)$ behaves like W is a small neighbourhood around the branch cut.

Say we instead let our function $g(x)$ be an elementary trigonometric function, as this introduces periodicity. Begin by letting $g(x) = \sin x$, which results in the inverse function $\mathfrak{B}(x) = \arcsin(W(x))$. As we are adding a periodic function, \mathfrak{B} will no longer shoot off to infinity. What we lose with this is replaced by the addition of another type of branch via the arcsin function. For $l \in \mathbb{Z}$, any real branch of $\mathfrak{B}(x) = \arcsin(W(x))$ can be expressed by the equation

$$\mathfrak{B}_\ell(x) = \arcsin_0((-1)^\ell W(x)) + \ell\pi \tag{4.1}$$

where $\arcsin_0(x)$ is the principal branch of arcsine, defined on the interval $[-1, 1]$.

This function is, in all reality, a doubly-indexed multivalued function. However, any branches which arise from composing arcsin with non-principal branches of $W_k(z)$ will result in values on the complex plane. Utilizing Riemann surfaces shows this in more detail. For \arcsin_0 , let the branch number of W_k vary. In 4.1, each ‘‘charisma’’¹ of some given $\mathfrak{B}(z)$ broadly

¹This term was pinned by my MSc advisor, Dr. David Jeffrey, to describe the Riemann surface for individual branches of multifunctions.

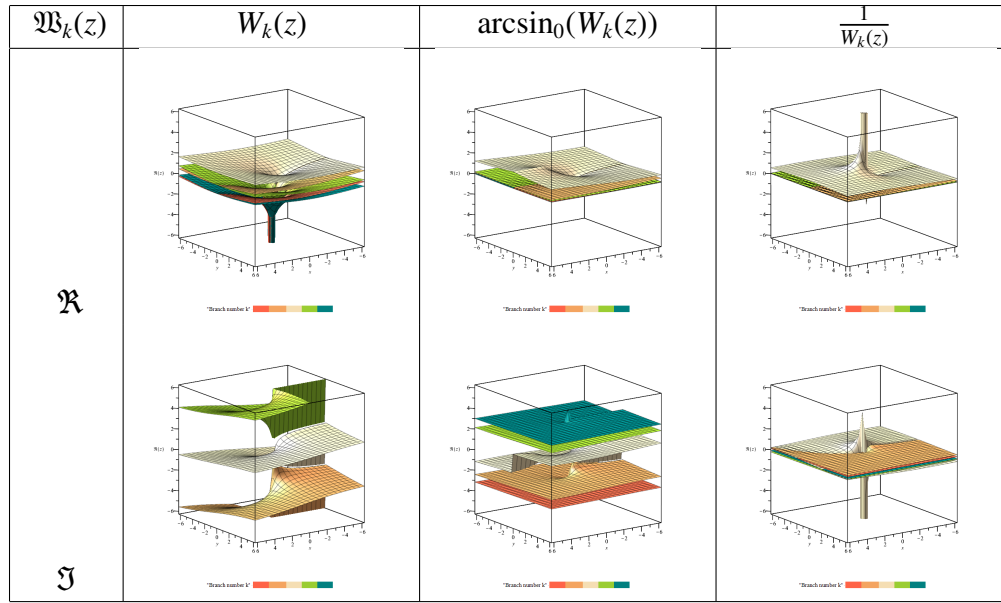


Table 4.1: Riemann surfaces for different $\mathfrak{B}_k(z)$, with the branches colored separately to denote branch number from $k = -2$ to $k = 2$.

resembles corresponding charisma of the nested $W_k z$. As it is quite difficult to distinguish the Riemann surfaces between some branches, it is also worth looking at the two-dimensional branch structure for elements of \mathfrak{Q} . For $W_k(z)$, the branch structure is defined parametrically by $z = it - t \cot t$. Thus, the branch structure of $\mathfrak{B}_k(z)$ can be defined as $z = g^{-1}(it - t \cot t)$. In this parametric equation, g^{-1} is the inverse of the function that appears in $f(z) = g(z)e^{g(z)}$. A couple of examples are plotted in figure 4.3.

4.2 The Fundamental Relation and The Lambert Family

Much like how the properties of inverse functions were exploited in the previous section, it can be shown that any element of \mathfrak{Q} will also obey the fundamental relation (1.5). A convenient consequence of this generalization is that series expansions of any $\mathfrak{B} \in \mathfrak{Q}$ will be easy to obtain, which is the focus of chapter 5. Though what follows is not a rigorous proof, it will be sufficient in extending the usage of (1.5).

Take the expression $g(z)e^{g(z)}$, where g is an invertable function over \mathbb{C} . Then, the function $(g^{-1} \circ W_k)(z) = \mathfrak{B}_k(z)$ is the solution to the equation

$$\mathfrak{B}_k(z)e^{\mathfrak{B}_k(z)} = z \tag{4.2}$$

This equation also obeys the fundamental relation. To show this, we may approximate $\mathfrak{B}_k(z) \approx g^{-1}(\ln_k z + p + u)$. By substituting this into the previous equation, we obtain what gives rise to the fundamental relation from before.

$$\begin{aligned} \mathfrak{B}(g^{-1}(\ln_k z + u))e^{\mathfrak{B}(g^{-1}(\ln_k z + u))} &= z \\ \implies z(\ln_k z + u)e^u &= z \end{aligned}$$

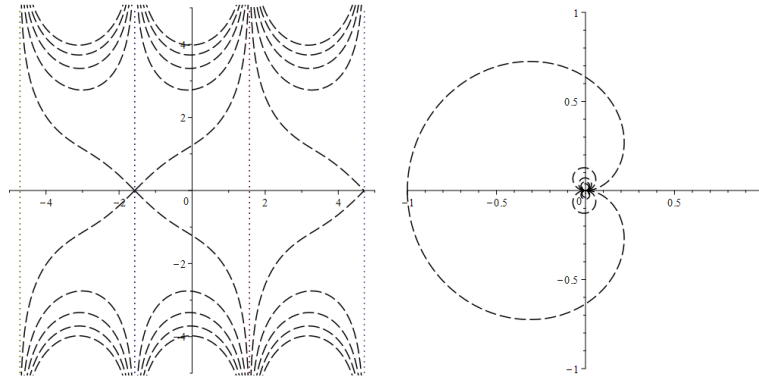


Figure 4.3: Branch structures for $\mathfrak{B} \in \mathfrak{L}$ over \mathbb{C} . $\mathfrak{B}_{\{k,\ell\}}(z) = \arcsin_{\ell}(W_k(z))$ is pictured on the left, $\mathfrak{B}_k(z) = \frac{1}{W_k(z)}$ on the right. On the left, arcsine branches are separated by dotted lines, and $W_k(z)$ branches are conversely distinguished by dashed lines.

Chapter 5

Asymptotic Series Expansions for Members of \mathfrak{L}

As the fundamental relation has been generalized to any function $\mathfrak{B}_k(z) \in \mathfrak{L}$, our new goal is to investigate the resulting series expansions. There are several ways to go about this task. First, a naive approach where we let the inverse nesting function $g^{-1}(z)$ act upon an asymptotic expansion $W_k^*(z)$. We can also nest approximations as a method of understanding how different types of series interact. Though the first approach can be utilized as a tool for extending previous findings, the second method is more appropriate for numerical analysis of series.

Similar to previous chapters, there will be a focus on members of \mathfrak{L} which compose elementary functions with $f(z) = ze^z$. However, it is crucial to also look into $\mathfrak{B}_k(z)$ which compose $W_k(z)$ with other special functions. Said special functions include $W_k(z)$ itself and the Jacobi elliptic integrals. Tools for this analysis broadly resemble the ones from Chapter 2, where the effects of varying N and p on images of domain curves are most nascent.

5.0.1 A Naive Approach

Establishing how the convergence properties of some $W_k^*(z)$ will carry over to a corresponding $\mathfrak{B}_k^*(z)$ is vital to understanding approximations of any $\mathfrak{B}_k(z)$. The inverse nesting function $g^{-1}(z)$ will not fundamentally change the convergence of the interior expansion $W_k^*(z)$; on the real plane, the approximation will consistently converge on the interval determined by p as $N \rightarrow \infty$. Though this forgoes deeper investigation into how series interact, it establishes a baseline approximation for the corresponding $\mathfrak{B}_k(z)$. As such, we start our analysis by simply composing a function with an asymptotic approximation of $W_k(z)$.

Start by defining $\mathfrak{B}_k(x) = \frac{1}{W_k(x)}$. On the real plane, this function has only two branches as the reciprocal function is single-valued. As was hinted to before, the approximations of $\mathfrak{B}_0(x)$ will be convergent on the interval $[e, \infty)$ for sufficiently large N and $p = 0$. Checking this for increasing N shows that this is the case in figure 5.1. Similarly, adjusting the value of p shows that, for $N = 10$, extended accuracy can be achieved by using $p = 6$ in $W_0^*(x)$.

An important detail of this specific case is the lack of convergence to the negative component of the principal branch. Though an approximation with $N = 10$ and $p = 6$ already showcases greatly improved convergence over smaller positive values, the other partition of the principal branch sees no improvement. Increasing N and p together will further improve

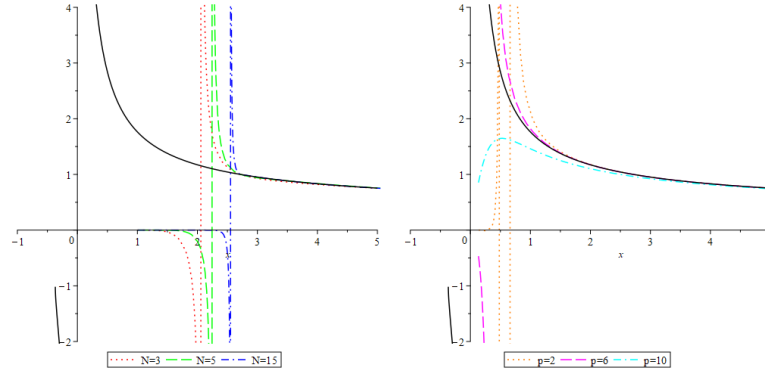


Figure 5.1: Approximations of $\mathfrak{W}_0(x) = \frac{1}{W_0(x)}$ with independent variations of N and p using (1.7). On the left, $p = 0$ and on the right, $N = 10$.

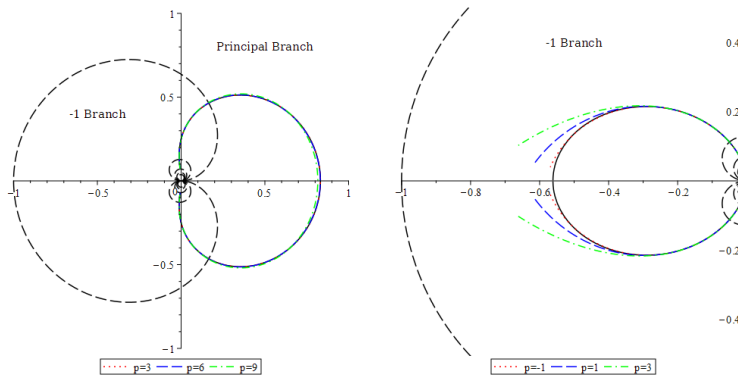


Figure 5.2: Approximations of images under $\mathfrak{B}_k(z) = \frac{1}{W_k(z)}$ using (1.10) and (2.15) with (1.7), respectively. On the left, $r = 4$. $r = 0.3$ on the right.

convergence for $x > 0$ at the cost of more computer storage, but convergence for $x < 0$ is still tenuous.

Over \mathbb{C} , the results will be much the same. To exploit the time-and-storage-saving properties of p , the following portion of this section will utilize graphs of $N = 10$ and varying values of p to showcase various $\mathfrak{W}_k^*(z)$ for large z . For sufficiently small z , values around $p = 1$ are used. Using images of circles, the properties of the approximations are preserved. The images are continuous at branch cuts and show greatest error near the principal branch cuts.

These asymptotic expansions will retain their properties and results for more complicated functions as well. Straight away, this can be shown for simple trigonometric functions. Each equivalent branch of $\arcsin_\ell(z)$ will retain the shape of the images in \mathbb{C} . However, one must have a sufficiently large value for p while approximating the principal branch in \mathbb{R} . Otherwise, $W_0^*(x)$ only starts to converge at $x = 1$. This is due to $W_0^*(x)$ falling outside the domain of $\arcsin(x)$ as $N \rightarrow \infty$ for $p = 0$ on the x -axis. In figure 5.3, the sine and cosine cases of $\mathfrak{W}_{\{k,\ell\}}^*(C)$ are plotted in \mathbb{C} , where C is a circle of radius $r = 1$. Utilizing larger values of p , we already see improved convergence in the principal branch.

The results for the trigonometric cases are repeated when elliptic integrals are introduced, albeit with branches repeating in two directions. The most basic function in this class is the in-

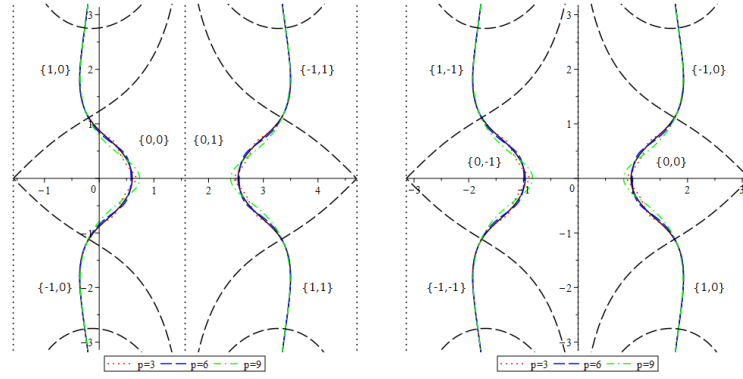


Figure 5.3: Approximations of $\mathfrak{B}_{(k,\ell)}(z)$ for the sine and cosine cases in \mathbb{C} , respectively. Here, the images are of a circle of radius $r = 1$ using the series (1.7).

complete elliptic integral of the first kind, $F(x|m)$, which is the inverse to the function $\text{sn}(x|m)$ ¹. This is also known as the elliptic sine, where m is a parameter called the modulus. The elliptic sine function itself is a doubly-periodic function whose periods are integer-multiples of the complete elliptic integral of the first kind, $K(m)$.

$$K(m) = \int_0^1 \frac{ds}{\sqrt{1-s^2} \sqrt{1-m^2s^2}} \quad (5.1)$$

Thus, the doubly-indexed inverse can be defined as followed:

$$F_{\{\ell,j\}}(z|m) = \int_0^z \frac{(-1)^\ell ds}{\sqrt{1-s^2} \sqrt{1-m^2s^2}} + 2\ell K(m) + 2jiK'(m); \ell, j \in \mathbb{Z} \quad (5.2)$$

The trigonometric form of $F(x|m)$ should also be mentioned, as it will be necessary in the next section:

$$F(\varphi, k) = \int_0^\varphi \frac{1}{\sqrt{1-(k \sin(\theta))^2}} d\theta \quad (5.3)$$

Here, φ is called the amplitude, defined in relation to z by $z = \sin(\varphi)$.

As with the trigonometric functions, the structure of the images of circles is preserved between all branches. This behaviour will still be observed when varying m . As $m \rightarrow 0$ $\text{sn}_{\{\ell,j\}}(z|m)$ degenerates into $\sin_\ell(z)$, $\mathfrak{B}(z)$ becomes the doubly-indexed case from before. So far, only functions with trivial relations between branches (or singular-valued functions) have been used. To add another layer of complexity, let the function acting upon W be another multifunction whose branches are not connected in an elementary fashion. One such function is the Lambert W function itself.

In this case, \mathfrak{B} will be a doubly-indexed multifunction whose branch structure will be the branches of $W_k(z)$ nested inside each individual branch of $W_\ell(z)$, so the images will vary drastically between branches. Though the images will change depending on the branch, the convergence properties of $W_k^*(z)$ will be retained. In figure 5.3, this is shown to be the case over \mathbb{C} .

¹The notation-related choice of writing $(x|n)$ is done merely to distinguish the form of the integral being used.

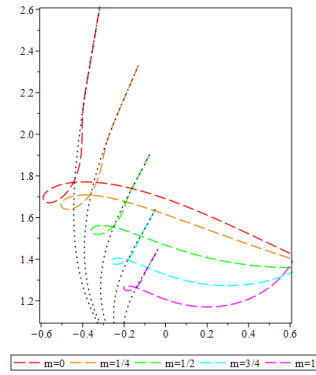


Figure 5.4: Approximations of $\mathfrak{B}_{\{0,0,0\}}(z|m) = F_{\{0,0\}}(W_0(x)|m)$ for various values of the modulus m in \mathbb{C} . The images are of a circle of radius $r = 0.8$ using (1.7), with each approximation (in color) set against their respective expected image (in black).

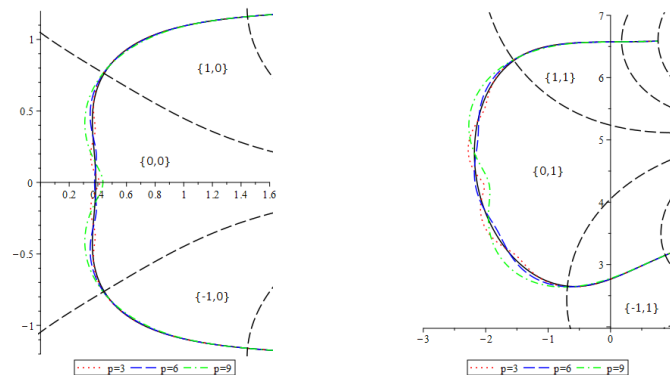


Figure 5.5: Approximations of $\mathfrak{B}_{\{k,\ell\}} = W_\ell(W_k(z))$ over \mathbb{C} using images of a circle of radius $r = 1$ and the approximation (1.7).

5.0.2 Accuracy and Efficiency of Nested Series

In addition to having some function $g^{-1}(z)$ act upon one of the previous approximations $W_k^*(z)$, nesting series of the two functions serves as a mode of studying approximations of \mathfrak{B} as well. Any choice of $g^{-1}(z)$ which acts upon W in the corresponding \mathfrak{B} may have its own Maclaurin, Taylor or asymptotic series which interacts with the asymptotic approximations for W . Compared with the previous section, they will be more expensive to compute as more terms are being generated. However, they allow for a space where the accuracy of purely series-based approximations can be studied.

The Reciprocal Function

An analysis of this method would benefit from a treatment similar to the previous section. Hence, let the nesting function $g^{-1}(z)$ start simple and progressively increase in complexity. Though we could utilize a fresh set of functions, attacking the topic of nested series in the same order as before will work just as well. First, let $g^{-1}(z) = \frac{1}{z}$. This function itself has a power series representation in the form of:

$$\frac{1}{z} = \lim_{M \rightarrow \infty} \sum_{a=0}^M (-1)^a (z-1)^a, |z-1| < 1 \quad (5.4)$$

Nesting this series with $W_k^*(z)$ admits a new approximation for $\mathfrak{B}_k(z) = \frac{1}{W_k(z)}$.

$$\frac{1}{W_k(z)} = \lim_{M \rightarrow \infty} \lim_{N \rightarrow \infty} \sum_{a=0}^M (-1)^a \sum_{n=1}^N \sum_{m=1}^n (\ln_k(z) - \ln_k(\ln_0(z)) + u_{n,m} - 1)^a \quad (5.5)$$

This approximation converges on the interval $[P, 2e^2]$ in \mathbb{R} , where P is determined by the choice of p . Letting $N = 10$ and $p = 6$ again, plotting the series over \mathbb{R} reveals an incidental feature of the approximation for smaller values of M . Though the series will converge to the naive method as M increases, a smaller number of terms M tends closer to the expected values of $\mathfrak{B}_0(x)$. To show this distinction, figure 5.6 has unconstrained axes to exaggerate the horizontal displacement between approximations.

This artifice of convergence appears over \mathbb{C} as well. For smaller values of M on the principal branch, the approximations tend closer to the actual result near smaller values of z . However, larger values of M cause the approximation to converge to the naive method as they did in \mathbb{R} . Another detail to note is that, as apposed to the naive method, the nested series does not approximate any other branches of $\mathfrak{B}_k(z)$ when $N = 10$ and $p = 6$. This can be seen in 5.7, and is due to non-principal branches of $W_k^*(z)$ lying outside the region of convergence of (5.4) for all z .

Trigonometric Functions

For trigonometric functions, there is a cache of approximations to choose from. As with the reciprocal case of \mathfrak{B} , these will endow the nested functions with their benefits and deficits. For

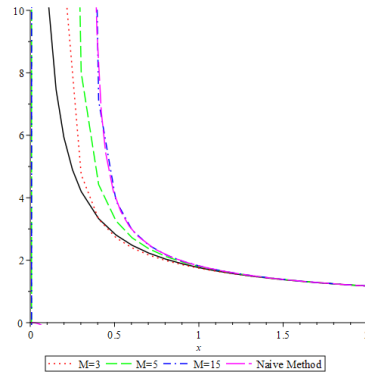


Figure 5.6: A nested series approximation of $\mathfrak{B}_0(x) = \frac{1}{W_0(x)}$ for various numbers of terms M using (1.7) and (5.4). $N = 10$ and $p = 6$.

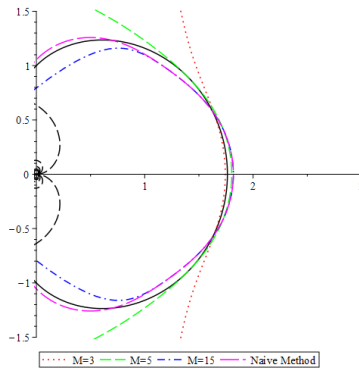


Figure 5.7: The analog to figure 5.6 in \mathbb{C} , showing the divergence of the nested series for larger values of z .

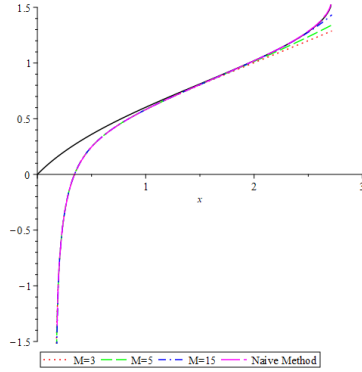


Figure 5.8: Real nested approximations of $\mathfrak{B}_{\{0,0\}}(0) = \arcsin_0(W_0(x))$ for different numbers of terms M . Here, we are using (1.7).

$\arcsin_\ell(x)$, there is the power series representation of the form

$$\arcsin_0(z) = \lim_{M \rightarrow \infty} \sum_{a=0}^M \frac{2a!}{(2a+1) \cdot (2^a a!)^2} z^{2a+1}, |z| < 1 \quad (5.6)$$

As opposed to the series expansion of $\frac{1}{x}$, this series approximation converges on the interval $[-1, 1]$. In \mathbb{R} , $\arcsin_\ell(x)$, $\ell \in \mathbb{Z}$ is only defined on that same interval for any branch ℓ . Thus, the nested series approximation

$$\arcsin_\ell(W_k(z)) = \lim_{M \rightarrow \infty} \lim_{N \rightarrow \infty} \sum_{a=0}^M \sum_{n=1}^N \sum_{m=1}^n \frac{(-1)^{2a+\ell+1} 2a!}{(2a+1) \cdot (2^a a!)^2} (\ln_k(z) - \ln_k(\ln_0(z)) + u_{n,m})^{2a+1} \quad (5.7)$$

will only converge in the annular region $|z| < e$. However, the series also can only converge in the region $|z| > e$ due to the asymptotic approximation of W . This means that, much like the reciprocal case, the series will not converge anywhere unless we use a non-zero value for p .

This is immediately reflected in figure 5.8, which plots $\mathfrak{B}_{\{k,\ell\}}^*(x) = \arcsin_\ell(W_k(x))$ over \mathbb{R} . With $N = 10$ and $p = 6$, the approximations rapidly converge to the naive approximation as M increases. Setting $p = 0$, there is no convergence over the entire real axis. A peculiar detail to note here is that, while the naive method receives numerical results faster in Maple, plots over \mathbb{R} generate quicker using the nested approximation.

Though the interval of convergence does not pose an issue in \mathbb{R} once a suitable p is chosen, it presents a problem in \mathbb{C} . Plotting the same approximations for a circle of radius $r = 1$ in figure 5.9 reveals that the nested series only approximates the principal branch. The strange occurrence of the nested plot processing faster does not carry over to \mathbb{C} either. To remedy this divergence outside the region $|z| < e$, instead use the asymptotic approximation of $\arcsin_0(z)$ adapted from Wolfram's function database [23].

$$\arcsin_0(z) = \frac{z}{2\sqrt{-z^2}} (\ln_0(-4z^2) - \sum_{a=1}^{\infty} \frac{(\frac{1}{2})_a z^{-2a}}{aa!}), |z| > 1 \quad (5.8)$$

Here, the expression $(\frac{1}{2})_a$ is the falling factorial.

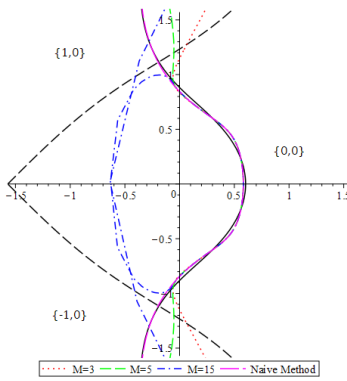


Figure 5.9: In \mathbb{C} , the prior approximation does not work as well outside of the principal branch.

The nested series will now converge over region $|z| > e$, which immediately reduces its efficacy over \mathbb{R} . However, this new nested series is significantly more viable in \mathbb{C} . Numerical computations for the value of circles of various radii at $\theta = \frac{\pi}{4}$ reveal improved convergence for larger z when using (1.7).

Approx.	Actual	(5.6)	(5.8)
$r = 1$	$0.51796 + 0.32236i$	$0.51796 + 0.32236i$	$57.44165 + 284.66003i$
$r = 2$	$0.80180 + 0.50176i$	$0.80576 + 0.50648i$	$0.95174 + 0.37443i$
$r = 3$	$0.96798 + 0.66421i$	$0.93853 + 0.56976i$	$1.06515 + 0.63378i$
$r = 4$	$1.06254 + 0.79881i$	$-3.85739 - 3.57794i$	$1.12423 + 0.79402i$
$r = 5$	$1.11979 + 0.90486i$	$-120.75376 - 41.20515i$	$1.16185 + 0.90754i$

² However, the goal of introducing a significantly more complicated expansion was to also approximate non-principal branches over \mathbb{C} . How well does the new nested series work? Using the same input values for the $k = 1$ branch of W reveals significant improvement over (5.6).

Approx.	Actual	(5.8)
$r = 1$	$-0.3114514153 + 2.395873006i$	$-0.3114557123 + 2.395759954i$
$r = 2$	$-0.1819677714 + 2.388373026i$	$-0.1818759992 + 2.388355000i$
$r = 3$	$-0.1818759992 + 2.388355000i$	$-0.2096472982 + 3.165540976i$

Jacobi Elliptic Functions and Nested Lambert W

Delving back into special functions serving as the nesting function within a given $\mathcal{B}_k(z)$, caution must be taken as certain functions have rather complicated series. Specimens such as Bessel functions and Legendre polynomials contain gamma functions and binomial coefficients in their series representations, but are still relatively small. They are merely teetering on the precipice of complexity; other special functions have significantly more cumbersome representations that do not justify the use of nesting series over the naive method.

The incomplete elliptic integral of the first kind $F(x|m)$ is one function whose expansions test this method's justification. In, [26] Campbell defines a series approximation for the com-

²To fit the width of this paper, the approximations have been taken to 5 decimal places.

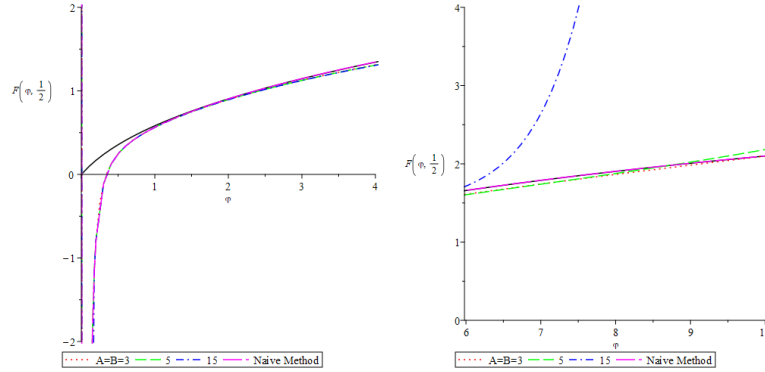


Figure 5.10: On the real principal branch of $\mathfrak{B}(\varphi, \frac{1}{2}) = F_{\{\ell,j\}}(W_k(\varphi), \frac{1}{2})$, the nested series converges to the naive method for small A and B when using (1.7).

plete elliptic integral of the first kind for any modulus m :

$$K(\sqrt{m}) = \sum_{a=0}^{\infty} \frac{2}{2a+1} P_a(2m-1) \quad (5.9)$$

Here, P_n is a Legendre polynomial. Though this can be used to shift between branches of $F_{\{\ell,j\}}(z|m)$, the trigonometric form of F has the following expansion, taken from [24]:

$$F_{\{0,0\}}(\varphi, m) = \lim_{A \rightarrow \infty} \lim_{B \rightarrow \infty} \varphi + \sum_{a=1}^A \sum_{b=1}^B \sum_{c=0}^{b-1} \frac{(\frac{1}{2})_b \binom{2b}{c} (-1)^{a+b-c} 2^{2a-2b+1} (c-b)^{2a} m^b}{b!(2a+1)!} \varphi^{2a+1} \quad (5.10)$$

This expansion converges to $F(\varphi, m)$ in the region $|\varphi| < 1$, or $|z| < \frac{\pi}{2}$. Thus, the resulting nested series representation for $\mathfrak{B}_{\{k,0,0\}}$ will converge over the annular region $a < |\varphi| < e$ in \mathbb{C} .

Though this series is rather complicated, it is surprisingly efficient when approximating the corresponding $\mathfrak{B}_{\{k,\ell,j\}}(\varphi, m) = F_{\{\ell,j\}}(W_k(\varphi), m)$. Utilizing (5.10) for the real principal branch reveals that $\mathfrak{B}_{\{k,\ell,j\}}^*(\varphi, m)$ converges for a relatively small number of terms. On \mathbb{R} , the distinction between approximations of $A = B = 3, 5$ and 15 is not made apparent until well after $\varphi > e$. In fact, figure 5.10 needs to have unconstrained axes to show this distinction. On the principal branch $\{0, 0, 0\}$ in \mathbb{C} , similar results are produced for the images of a circle of radius $r = 1$. As the series diverges near branch cuts of $W_k(z)$, only the principal W branch sees convergence of the nested series.

Due to this, it may be tempting to use an asymptotic approximation for $F(\varphi, m)$ as we did for arcsine. Quickly referencing Wolfram's function database [25] again shows that this task falls off the edge into unnecessary complexity. Returning to the path of the last section, nesting series representations of W with itself is a markedly more straightforward task. Set $g^{-1}(z) = W_\ell(z)$ such that $\mathfrak{B}_{\{k,\ell\}}(z) = g^{-1}(W_k(z)) = W_\ell(W_k(z))$. Straight away there are already two types of approximations for this function, utilizing Taylor and asymptotic expansions respectively.

$$\mathfrak{B}_{\{0,0\}}(x) = \lim_{N \rightarrow \infty} \sum_{n=1}^N (-n)^{(n-1)} \frac{(W_k^*(z))^n}{n!} \quad (5.11)$$

$$\mathfrak{B}_{\{k,\ell\}}(z) = \ln_\ell(W_k^*(z) - \ln_0(q + \ln_\ell(W_k^*(z)))) + u(W_k^*(z)) \quad (5.12)$$

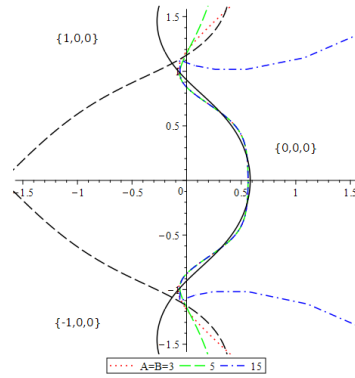


Figure 5.11: The images of a circle of radius $r = 1$ under the same nested series approximation of $\mathfrak{B}(z)$ in \mathbb{C} .

For the asymptotic approximation of the outer $W_\ell(z)$, M represents the number of terms and q will be its equivalent of p .

Some combinations of these series will not be compatible. For example, the asymptotic series converges on $|z| > e$. However, $W_0(e) = 1$, which lies outside the disc where the Taylor series converges. Conversely, it is not productive to nest the Taylor series within the asymptotic series for the same reason. Set $N = M = 10$ and $p = q = 6$ for the double asymptotic and Taylor approximations. Performing some numerical experiments on the principal branch $\{0, 0\}$, the series work as intended.

Approx.	Actual	(5.12)	(5.11)
$x = 0.1$	0.08392849326	$0.763667512 + 1.946141996i$	0.08392848685
$x = 1$	0.3856588411	0.292661907	$-1.917421339 \times 10^{25}$
$x = e$	0.5671432904	0.5503190697	$-4.315820393 \times 10^{69}$

The double asymptotic nested approximation also performs well for large values of z on non-principal branches. To save on computational cost, $N = M = 5$ and $p = q = 3$. Taking a circle of radius $r = 1$, test the series at $\theta = \frac{\pi}{2}$ for various branches $\{k, \ell\}$:

Approx.	Actual	(5.12)
$\{0,0\}$	0.3856588411	0.221002047
$\{1,0\}$	$1.090550373 + 1.112595928i$	$1.093629601 + 1.097310628i$
$\{1,1\}$	$-0.3495901090 + 6.567206636i$	$-0.3483494787 + 6.566825783i$
$\{2,1\}$	$0.5144314992 + 6.580476820i$	$0.5147020294 + 6.581230717i$
$\{2,2\}$	$-0.1459094909 + 12.77422370i$	$-0.1458524964 + 12.77419438i$

5.0.3 Some Special Cases

To close out the chapter, there are a few special cases of $\mathfrak{B}(z)$ that are of particular interest. The functions that have been covered so far retain the branch structure of $W_k(z)$ itself. There has been a semblance of the original function which anchored each member of \mathfrak{Q} to $W_k(z)$, but this does not tell the whole story. Some functions in \mathfrak{Q} are more elementary functions, and some may not carry the aforementioned branch structure of $W_k(z)$ at all.

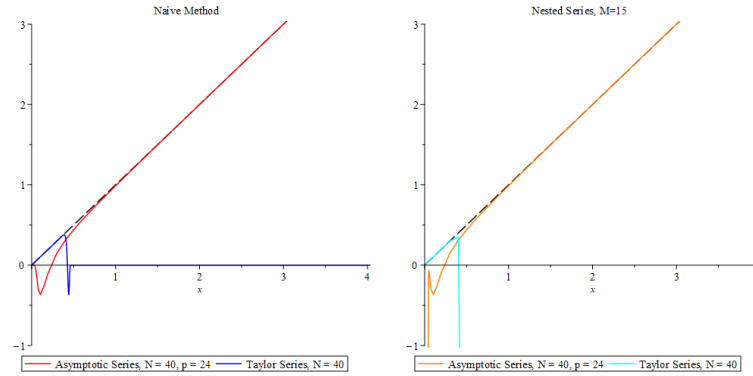


Figure 5.12: Naive and nested series approximations of $\mathfrak{B}(x) = x$ on \mathbb{R} using (1.7).

Going back to $\mathfrak{B}_k(x) = g^{-1}(W_k(x))$, letting $g^{-1}(x) = xe^x$ will return $\mathfrak{B}(x) = x$. Though trivial, this is an elementary function which does not preserve the branch structure of $W_k(z)$. In fact, all branches will degenerate into a single branch under composition. There are, however, still series expansions for this $\mathfrak{B}(x)$ which arise from the methods covered earlier in the chapter. Define the series expansion for $g^{-1}(z) = ze^z$ as follows:

$$ze^z = \lim_{M \rightarrow \infty} \sum_{m=0}^M \frac{x^m}{(m-1)!} \quad (5.13)$$

This series converges for all z as $M \rightarrow \infty$. How will the different branches affect the accuracy of corresponding $\mathfrak{B}^*(z)$? Furthermore, how accurately can the identity function be approximated with the previous series?

Over \mathbb{R} , the same results play out for both the naive and nested series methods. Though most of $\mathfrak{B}(x) = x$ can be approximated with either the Taylor or asymptotic expansions of $W_0(x)$, there is a gap between the two approximations. Of most interest is the behaviour in the non-convergent regions of x for both the Taylor and asymptotic series in the naive method. As plotted in figure 5.12, the nested series diverge asymptotically. However, the naive method approximations start to diverge, but quickly go to $x = 0$ after reaching a minimum of $y = -\frac{1}{e}$.

On \mathbb{C} , the degenerated branch structure allows for a more nuanced aspect of approximation. As all the branches are together as one, different branch approximations in the series will give different approximations of the same image. Choosing to be repetitive, use images of a circle of radius $r = 1$ again. The image is itself, but the Naive method has imperfections similar to those highlighted before. The images in \mathbb{C} are plotted in figure 5.13. As reflected in said figure, the increased accuracy seen in $W_k^*(z)$ for any non-principal k admits higher accuracy for the same number of terms N and correction p .

The nested series has a more dubious time approximating the curve, however. Though the Taylor series of $g^{-1}(z) = ze^z$ converges for all z as $M \rightarrow \infty$, the series does not converge quickly for finite M . Thus, when plotting the nested series representation of z in figure 5.14, the images will wind around the naive method image before diverging.

The identity function is not the only \mathfrak{B} that eschews the branch structure of $W_k(z)$. Define $g^{-1}(z) = e^z$ such that $\mathfrak{B}_k(z) = e^{W_k(z)}$. This function is the inverse of the function $f(z) = z \ln_k(z)$. Though the branches have not degenerated like with the identity function, the branches of

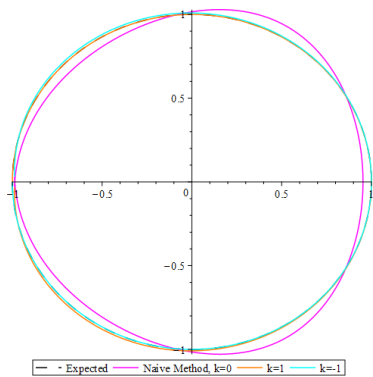


Figure 5.13: Naive approximations of a circle of radius $r = 1$ using $\mathfrak{B}^*(z)$ and (1.7). Here, $N = 10$ and $p = 6$.

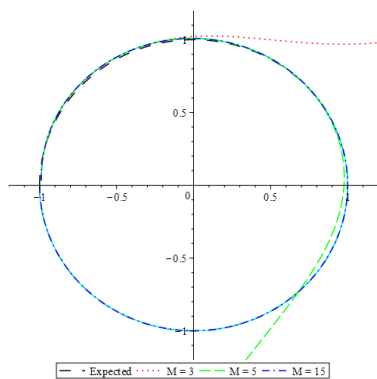


Figure 5.14: Nested series approximation of z for various terms numbers M of the ze^z Taylor series, where $W_k^*(z)$ is using (1.7). $N = 10$, $p = 6$ and $k = 1$.

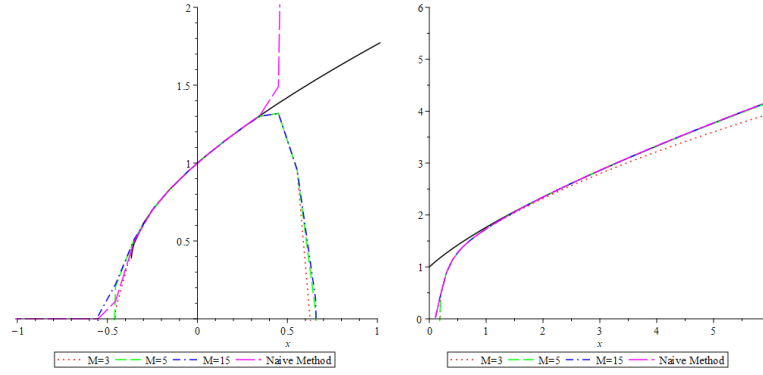


Figure 5.15: Comparisons of approximations of the principal branch of $\mathfrak{B}_0 = e^{W_0(x)}$ over \mathbb{R} . On the right, the Taylor series approximation of $W_0(x)$ at $x = 0$ is used. Similarly, the right image uses the asymptotic approximation with (1.7). Here, $N = 10$ and $p = 6$.

$\mathfrak{B}_k(z) = e^{W_k(z)}$ are not as neatly defined as with $W_k(z)$. In \mathbb{C} , each branch k and its conjugate branch $-k$ overlap with each other but are not equivalent. Branch continuity still exists between the images in each branch, but now images intersect with images in other branches.

Pulling back the complexity, the same methods from before can be used to approximate the real principal branch of the corresponding $\mathfrak{B}_k(z)$. Said principal branch is defined on the interval $[-\frac{1}{e}, \infty)$, with a branch cut at $(x, y) = (-\frac{1}{e}, \frac{1}{e})$ shared with the -1 branch. Using the Taylor series for e^z

$$e^z = \lim_{M \rightarrow \infty} \sum_{m=0}^M \frac{z^m}{m!} \quad (5.14)$$

which converges for all z as $M \rightarrow \infty$, the only limitations of $\mathfrak{B}_0^*(x)$ will be the limitations of $W_0^*(x)$. Plotting naive and nested series approximations in figure 5.15, the results for all the other examples are reflected yet again.

Chapter 6

Conclusion

Though this coverage has not been exhaustive, it is meant as a starting point for the numerical analysis of non-elementary functions. These functions fill a strange niche in the realm of mathematics, seemingly violating the definition of a function when considered in its entirety. The Lambert W function itself is a stranger among strangers in this regard, as its branches are not related in a trivial fashion. However, years of research have already lent us a comprehensive understanding of W . This thesis is meant to supplement and add upon our knowledge of W through the applications it has discussed.

This thesis has discussed ways to expand the uses of asymptotic approximations of the Lambert W function. First, we focused on generalizing previously established series to any $W_k(z)$ in \mathbb{C} for $k \in \mathbb{Z}$. Additionally, the accuracy of generalizations was discussed and a new series was posed to approximate non-principal branches at small z . A new family of functions was introduced as well, and prior approximations were used to estimate individual members of this family. This concluded with a short analysis of members which arise from more elementary functions.

Looking forward, a future goal of related research is a more comprehensive look at \mathfrak{W} . The nesting functions used cover a handful of properties, but there was limited consideration of periodic functions. Additionally, there are other multivalued functions which exhibit non-trivial branch cuts. An example from astrophysics is the inverse of Kepler's law, where the branches of the eccentric anomaly are determined by the eccentricity of the orbit. Multivalued functions are a field still open to generalization and analysis, and this is merely an exploration of these aspects.

Bibliography

- [1] R. M. Corless, G. H. Gonnet, D. E. G. Hare, D. J. Jeffrey, D. E. Knuth. On the Lambert W function. *Adv. Comp. Math.*, 5(4):329–359, 1996.
- [2] D. J. Jeffrey, D. E. G. Hare, and R. M. Corless. Unwinding the branches of the Lambert W function. *Math. Scientist*, 21:1–7, 1996.
- [3] W. Kahan. Branch cuts for elementary functions. In *The state of the art in numerical analysis*, ed M.J.D. Powell and A. Iserles, Oxford.
- [4] F. W. J. Olver, A. B. Olde Daalhuis, D. W. Lozier, B. I. Schneider, R. F. Boisvert, C. W. Clark, B. R. Miller, B. V. Saunders, H. S. Cohl, and M. A. McClain, eds. NIST Digital Library of Mathematical Functions. <https://dlmf.nist.gov/>, Release 1.1.10 of 2023-06-15.
- [5] P. Flajolet, D. E. Knuth, B. Pittel. The first cycles in an evolving graph. *Discrete Mathematics*, 75:167–215, 1989.
- [6] J. M. Borwein, S. B. Lindstrom. Meetings with Lambert W and other special functions in optimization and analysis. *Pure and Applied Functional Analysis* 1.3:361–396, 2016.
- [7] G. A. Kalugin, D. J. Jeffrey, R. M. Corless, P. B. Borwein. Stieltjes and other integral representations for functions of Lambert W . *Integral Transforms & Special Functions*, 23(8):581–593, 2012.
- [8] R. Iacono, J. P. Boyd. New approximations to the principal real-valued branch of the Lambert W -function. *Advances in Computational Mathematics*, 43:1403–1436, 2017.
- [9] O. A. R. Mahroo1, T. D. Lamb. Recovery of the human photopic electroretinogram after bleaching exposures: estimation of pigment regeneration kinetics. *Journal of Physiology*, 554.2:417–437, 2004.
- [10] G. Marsaglia, J. C. W. Marsaglia. A new derivation of Stirling’s approximation to $n!$. *American Math. Monthly* 97(9):826–829, 1990.
- [11] V. Vinogradov. On Kendall–Ressel and related distributions. *Statist. Probab. Lett.* 81:1493–1501, 2011.
- [12] V. Vinogradov. Some utilizations of Lambert W function in distribution theory. *Commun. Stat. Theory Methods*, 42:2025–2043, 2013.
- [13] N. G. de Bruijn. *Asymptotic Methods in Analysis*. North-Holland, 1961.

- [14] R. M. Corless, D. J. Jeffrey, and D. E. Knuth. A sequence of series for the Lambert W function. In Wolfgang W. Küchlin, editor, *ISSAC '97: Proceedings of the 1997 International Symposium on Symbolic and Algebraic Computation*, pages 197–204. Association of Computing Machinery, 1997.
- [15] D. J. Jeffrey and S. M. Watt. Working with families of inverse functions. In K. Buzzard and T. Kutsia, editors, *Intelligent Computer Mathematics*, volume 13467 of *Lecture Notes in Computer Science*, pages 1–16. Springer, 2022.
- [16] F. W. J. Olver. *Asymptotics and special functions*. Academic Press, 1974.
- [17] L. Comtet. Inversion de $y^\alpha e^y$ et $y \log^\alpha y$ au moyen des nombres de Stirling. *C. R. Acad. Sc., Paris*, 270:1085–1088, 1970.
- [18] R. L. Graham, D. E. Knuth, O. Patashnik. *Concrete Mathematics*, 2nd Ed. Addison–Wesley 1994.
- [19] R. B. Dingle. *Asymptotic expansions: their derivation and interpretation*. Academic Press, 1973.
- [20] M. M. Benghorbal. Power series solutions of fractional differential equations and symbolic derivatives and integrals. PhD Thesis, The University of Western Ontario, 2004.
- [21] D. J. Jeffrey, R. M. Corless, D. E. G. Hare, and D. E. Knuth. Sur l’inversion de $y^\alpha e^y$ au moyen des nombres de Stirling associés. *Comptes Rendus Acad. Sci. Paris Serie I-Mathematique*, 320(12):1449–1452, 1995.
- [22] G. A. Kalugin, D. J. Jeffrey Series transformations to improve and extend convergence. In Gerdt, V. P., Koepf, W., Mayr, E. W., Vorozhtsov, E. V., editors, *Computer Algebra in Scientific Computing. CASC 2010.*, volume 6244 of *Lecture Notes in Computer Science*, pages 134–147. Springer, 2010.
- [23] O. Marichev, M. Trott, eds., Wolfram Research, The Mathematical Functions Site. <http://functions.wolfram.com/01.12.06.0018.01>
- [24] O. Marichev, M. Trott, eds., Wolfram Research, The Mathematical Functions Site. <http://functions.wolfram.com/01.12.06.0018.01>
- [25] O. Marichev, M. Trott, eds., Wolfram Research, The Mathematical Functions Site. <http://functions.wolfram.com/08.05.06.0035.01>
- [26] J. M. Campbell, J. D’Aurizio, J. Sondow On the interplay among hypergeometric functions, complete elliptic integrals, and Fourier–Legendre expansions In Krantz, S. G., Chen, G., Aron, R. M., editors, *Journal of Mathematical Analysis and Applications*, 479(1):90–121, 2019.

Curriculum Vitae

Name: Jacob Imre

**Post-Secondary
Education and
Degrees:** The University of Toledo
Toledo, OH, USA
2017 - 2021 B.Sc.

University of Western Ontario
London, ON
2021 - 2023 M.Sc.

**Related Work
Experience:** Mathematics Tutor
The University of Toledo
2019 - 2021

Graduate Teaching Assistant
The University of Western Ontario
2021 - 2023

Publications:

J. Imre, D. J. Jeffrey. Non-principal Branches of Lambert W. A Tale of 2 Circles. In Boulier, F., England, M., Kotsireas, I., Sadykov, T.M., Vorozhtsov, E.V., editors, CASC 2023. Volume 14139 of *Lecture Notes in Computer Science*, pages 199-212. Springer, 2023.